

1 **Gibberellins promote polar auxin transport to regulate stem cell fate decisions in cambium**

2

3 Riikka Mäkilä^{1,2}, Brecht Wybouw^{1,2}, Ondrej Smetana^{1,2}, Leo Vainio^{1,2}, Anna Solé-Gil^{1,2}, Munan Lyu^{1,2}, Lingling
4 Ye^{1,2}, Xin Wang^{1,2}, Riccardo Siligato^{1,2,3}, Mark Kubo Jenness⁴, Angus S. Murphy⁴, Ari Pekka Mähönen^{1,2,*}

5

6 ¹ Organismal and Evolutionary Biology Research Programme, Faculty of Biological and Environmental
7 Sciences and Viikki Plant Science Centre, University of Helsinki, Helsinki, Finland.

8 ² Institute of Biotechnology, HiLIFE, University of Helsinki, Helsinki, Finland.

9 ³Present address: European Commission, Joint Research Centre, Retieseweg 111, 2440 Geel, Belgium

10 ⁴ Department of Plant Science and Landscape Architecture, University of Maryland, College Park, USA.

11 *Correspondence: AriPekka.Mahonen@helsinki.fi.

12

13

14 **Abstract**

15 Vascular cambium contains bifacial stem cells, which produce secondary xylem to one side and secondary
16 phloem to the other. However, how these fate decisions are regulated is unknown. Here, we show that the
17 positioning of an auxin signalling maximum within the cambium determines the fate of stem cell daughters.
18 The position is modulated by gibberellin-regulated, PIN1-dependent polar auxin transport. Gibberellin
19 treatment broadens auxin maximum from the xylem side of the cambium towards the phloem. As a result,
20 xylem-side stem cell daughter preferentially differentiates into xylem, while phloem-side daughter retains
21 stem cell identity. Occasionally, this broadening leads to direct specification of both daughters as xylem, and
22 consequently, adjacent phloem-identity cell reverts to being stem cell. Conversely, reduced gibberellin levels
23 favour specification of phloem-side stem cell daughter as phloem. Together, our data provide a mechanism
24 by which gibberellin regulates the ratio of xylem and phloem production.

25

26 **Main**

27 Vascular cambium is responsible for the lateral (secondary) growth of plant stems and roots. This process is
28 particularly prevalent in tree species but also occurs in non-woody species like *Arabidopsis thaliana*¹. The
29 vascular cambium consists of meristematic cells that undergo periclinal cell divisions (that is, cell divisions
30 parallel to the surface of the organ)². Cambium cells that leave the meristem ultimately differentiate into
31 parenchymatic or conductive cells, with secondary xylem being produced inwards and secondary phloem
32 outwards³ (**Extended Data Fig. 1a**). Recent lineage-tracing studies showed that a subset of cambial cells act
33 as bifacial stem cells, since a single cambial cell is capable of producing both xylem and phloem⁴⁻⁶.

34 A major regulator of cambium development is the phytohormone auxin^{4,7,8}. Mutations in genes encoding
35 components of auxin signalling including those associated with perception and polar transport of the
36 hormone cause defects in cambium development^{4,9}, vascular patterning^{4,9-11}, leaf venation¹², xylem and
37 phloem formation *in planta*^{4,13,14}, in tissue culture¹⁵ and during vascular regeneration¹⁶. Recently, we showed
38 that ectopic clones with high levels of auxin signalling force non-xylem cells to differentiate into secondary
39 xylem vessels, while cells adjacent to such clones divide periclinally and gain expression of cambial markers⁴.
40 The ectopic clone thus behaves as an organizer that causes adjacent cells to specify as vascular cambium
41 stem cell-like cells. In agreement with this, an auxin maximum is normally located on the xylem side of the
42 vascular cambium, and stem cell divisions occur adjacent to this maximum⁴. These data raise the question
43 whether the location of the auxin maximum within the cambium has a role in stem cell fate decisions.

44 Other phytohormones also influence cambium development alongside auxin⁸. For example, gibberellins (or
45 gibberellic acid, GA) promote secondary xylem production in both *Arabidopsis*^{17,18} and poplar¹⁸⁻²⁰. In
46 *Arabidopsis*, this occurs during flowering, when GA levels rise¹⁷. Recently, *AUXIN RESPONSE FACTORS 6* (*ARF6*)
47 and *ARF8* have been shown to mediate auxin-dependent xylem production that is downstream of GA²¹.
48 Interactions between auxin and GA also occur in other biological processes. For example, in *Arabidopsis*
49 roots, GA directly promotes abundance of PIN polar auxin transporters in the root meristem, thus regulating
50 polar auxin transport (PAT)²².

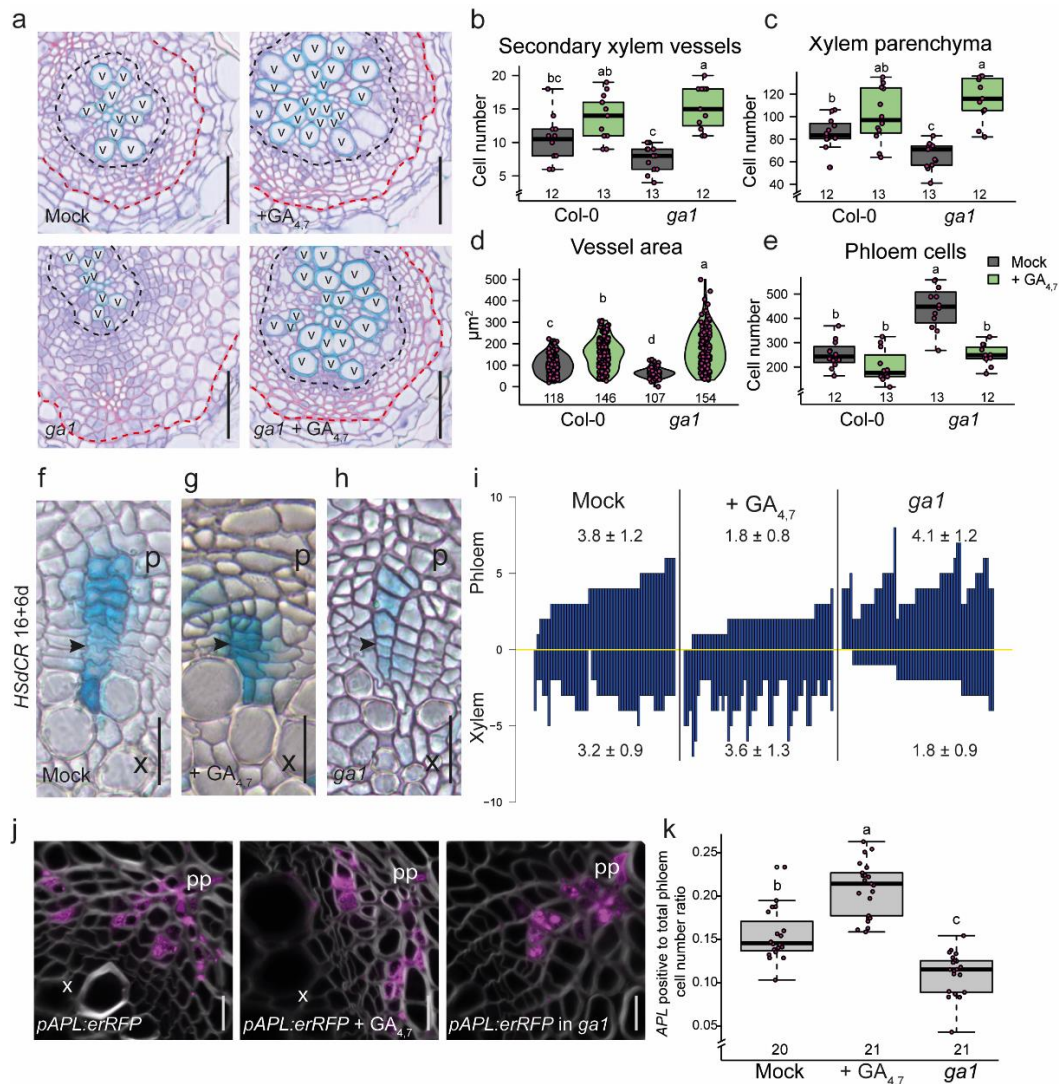
51 In this work, we show that GA promotes PIN1-dependent PAT in *Arabidopsis thaliana* roots. This results in an
52 expanded auxin signalling maximum within the root vascular cambium, which forces cambial stem cell
53 daughters to preferentially specify as xylem cells. Our data show how GA influence the position of the auxin
54 maximum in cambium, therefore determining stem cell fate decisions between xylem and phloem.

55

56 **GA regulates stem cell fate decisions**

57 Previously, GA has been shown to increase xylem formation in *Arabidopsis* hypocotyls during flowering¹⁷. In
58 order to understand the role of GA on cambial growth dynamics, we analysed GA's effect in *Arabidopsis* roots
59 at a cellular resolution. To reach that goal, we analysed roots during the early stages of secondary growth,
60 when cell division and differentiation dynamics are easier to follow. At these stages, only two types of xylem
61 cells are produced: secondary xylem vessels and xylem parenchyma (**Extended Data Fig. 1a**). Secondary
62 xylem vessels expand radially and deposit a thick secondary cell wall before fully differentiating into hollow,
63 water-conducting vessels, while xylem parenchyma remain in an undifferentiated state. As expected, GA
64 treatment in young roots resulted in an increased number of both secondary xylem vessels and xylem
65 parenchyma, and the increase was equal in both cell types (**Fig. 1a,b,c; Extended Data Fig. 1b**). In addition,
66 secondary xylem vessel expansion increased as a result of GA treatment (**Fig. 1a,d**). In contrast to plants
67 treated with GA, a mutant deficient in GA biosynthesis, *ga1*²³, had a reduced number of xylem vessels and
68 parenchymatic cells (**Fig. 1a,b,c**). Additionally, the xylem vessel area was reduced (**Fig. 1a,d**). All of these
69 phenotypes were rescued by GA treatment (**Fig. 1a,b,c,d**). Altogether, these data show that GA promotes
70 the production of both xylem vessels and parenchyma during the early stages of secondary growth in roots.

71 To investigate the mechanism causing the observed changes in xylem cell number, we looked for alterations
72 in the cambium growth dynamics. We used a previously established a heat shock inducible CRE-*lox* based
73 lineage-tracing system (*HsdCR*)⁴ which allows the production of single-cell clones within a population of
74 dividing cells, including cambium. This enabled us to monitor the cambium growth dynamics over time.
75 Under normal growth conditions, lineages are derived from a single recombination event in one stem cell
76 and span towards both the xylem and phloem side in an almost equal manner (**Fig. 1f,i**). This indicates that
77 bifacial stem cell divisions normally provide an equal number of new xylem and phloem cells. Under GA-
78 treated conditions, clone cell lineages show an unequal distribution (**Fig. 1g,i**), with a preference towards the
79 xylem side, while lineages in the *ga1* mutant background preferably span towards the phloem (**Fig. 1h,i**). We
80 did not observe proliferating sectors exiting the cambium and entering differentiating tissue in any of the
81 conditions (**Fig. 1i**). These data indicate that GA regulates stem cell fate decisions during cambium
82 proliferation rather than specifically regulating xylem or phloem proliferation.



83

84 **Figure 1. GA induces secondary xylem proliferation and vessel expansion.** (a) Root cross-sections after a 10-day GA
85 treatment in 4-day old Col-0 and *ga1* plants. Black dotted lines indicate the most recent cell divisions. Red dotted lines
86 mark the border between the phloem parenchyma cells and the periderm. (b-e) Quantifications of secondary vessel (b)
87 and xylem parenchyma cell numbers (c), individual secondary vessel area (d), and total phloem cell number (e) in 14-
88 day old seedlings. (f-i) Lineage tracing in active cambium with GUS stained sectors (blue) originating from a single
89 recombination event. Recombination was induced in 16-day old seedlings, after which the seedlings (Col-0 in f,g and
90 *ga1* in h) were grown for an additional 6 days under mock (f,h) or GA_{4,7} conditions (g). Black arrowheads indicate the
91 most recent cell divisions in the sectors, where the thinnest cell wall was observed. (i) GUS sectors (bars) plotted relative
92 to the position of the thinnest cell wall (yellow line) in each sector. Values above and below the bars indicate average
93 number of phloem and xylem cells (±SD), respectively, within the sectors. Some of the sectors, especially after GA
94 treatment, ended on xylem vessels, which are dead and thus cannot be observed with GUS staining. Therefore, the
95 length of these sectors towards the xylem is an underestimation of the actual length. (j) Confocal cross sections of
96 *pAPL:erRFP* after an 11-day GA treatment in 4-day old plants (except *pAPL:erRFP* in the *ga1* mutant background, which
97 was grown 15 days in Mock). The *APL* reporter marks conductive phloem cells. (k) The ratio of cells expressing *APL*
98 versus all phloem cells in j. In b,c,e and k, the boxes in the box and whisker plots show the median and interquartile
99 range, and the whiskers show the total range. Individual data points are plotted as purple dots. In the violin plots in d,
100 the white dot shows the median and the thick line the interquartile range. The thinner line represents the rest of the
101 distribution. Each side of the line is a kernel density estimation that shows the distribution shape of the data. Individual
102 data points are plotted as purple dots. Numbers in b-e and k indicate number of samples. Two-way ANOVA with Tukey's
103 post hoc test in b-e and k. Letters indicate a significant difference, *P* < 0.05. Scale bars are 50 μm (a), 20 μm (f-h) or 10
104 μm (j). "p" = phloem, "pp" = primary phloem pole, "x" = xylem "v" = secondary xylem vessel. All experiments were
105 repeated three times.

106

107 Dual function of GA on phloem formation

108 Previous histological studies in hypocotyl²¹ and our lineage-tracing results in root (Fig. 1i) show that GA
109 inhibits phloem production. Next, we tested whether GA affects the production of different phloem cell
110 types. Phloem consists of conductive cells known as sieve elements, together with their companion cells and
111 phloem parenchyma (**Extended Data Fig. 1a**). In agreement with the lineage-tracing results, total phloem cell
112 numbers were decreased in GA-treated roots and increased in the *ga1* mutant background (**Fig. 1a,e**). Next,
113 we used the conductive phloem cell specific marker *ALTERED PHLOEM DEVELOPMENT* (*APL*)²⁴ to determine
114 whether GA affects the number of conductive phloem cells. We observed that the ratio of APL-positive cells
115 to total phloem cells was increased after GA treatment and decreased in *ga1* (**Fig. 1j,k**). Thus, with excess
116 GA, plants produce more conductive phloem, and with limited GA, they instead produce parenchymatic cells.
117 Similar results were observed when quantifying the number of sieve elements by safranin staining²⁵; the
118 number of sieve elements was decreased in *ga1* (**Extended Data Fig. 1f,g**). These results seem
119 counterintuitive compared to the lineage tracing and total phloem number results, where the reverse
120 tendency was observed. We therefore analysed the overall expression pattern of *APL* in more detail. In *ga1*,
121 *APL* expression showed that phloem differentiation is more focused around the primary phloem pole regions
122 and is situated further away from the dividing stem cells than in normal conditions (**Extended Data Fig.**
123 **1c,d,e**). In contrast, after GA treatment, plants show broader *APL* expression, with phloem differentiation
124 occurring slightly closer to the dividing stem cells (**Extended Data Fig. 1d,e**). These data indicate that GA
125 inhibits a phloem fate decision by cambial stem cells; however, those few cells that do specify as phloem will
126 preferentially differentiate as conductive phloem.

127

128 GA signalling is required in the early xylem domain

129 Next, we wondered where and how GA affects cambium growth dynamics. First, we aimed to understand
130 which tissue types GA signalling operates in during secondary growth. DELLA proteins act as repressors of GA
131 signalling, and they are rapidly degraded in the presence of GA²⁶. Mutations in one of the DELLA genes,
132 *REPRESSOR OF GA* (*RGA*)²⁷, result in increased xylem area²¹ within the hypocotyl and could therefore also
133 have an effect in root secondary growth. Indeed, we found that *pRGA:GFP-RGA*²⁷ showed broad expression
134 in the root cambium, appearing in both the xylem and the phloem (**Fig. 2a**), and a 6 h GA application led to
135 degradation of the *pRGA:GFP-RGA* signal in all cell types (**Fig. 2a**), indicating that the GA signalling
136 components are broadly present in secondary tissues.

137 Deletion of 17 amino acids within the DELLA domain of RGA (*RGAΔ17*) results in the formation of a dominant,
138 non-degradable version of the protein²⁸. By driving this dominant inhibitor of GA signalling under three
139 different cell type-specific inducible promoters, we investigated where GA signalling is required for its effect
140 on cambium development. Inhibition of GA signalling under the promoter of the early phloem gene *PHLOEM-*
141 *EARLY-DOF 1* (*PEAR1*)²⁹ did not inhibit xylem production; unexpectedly, it led to an increase in xylem cell
142 number (**Fig. 2b,c,f**). However, *RGAΔ17* induction under the promoter of the stem cell gene
143 *AINTEGUMENTA* (*ANT*)⁴, and especially under the promoter of the early xylem gene *HOMEODOMAIN 8*
144 (*AtHB8*)⁴ significantly reduced xylem production (**Fig. 2b,d-f**), with the strongest lines resembling the *ga1*
145 mutant phenotype (**Fig. 1a** and **Fig. 2e**). These data indicate that GA signalling in the stem cells and in early
146 xylem is required for its role in promoting xylem production. This is also in accordance with measured
147 bioactive GA gradients within poplar stems²⁰, which show a GA maximum in the developing xylem.

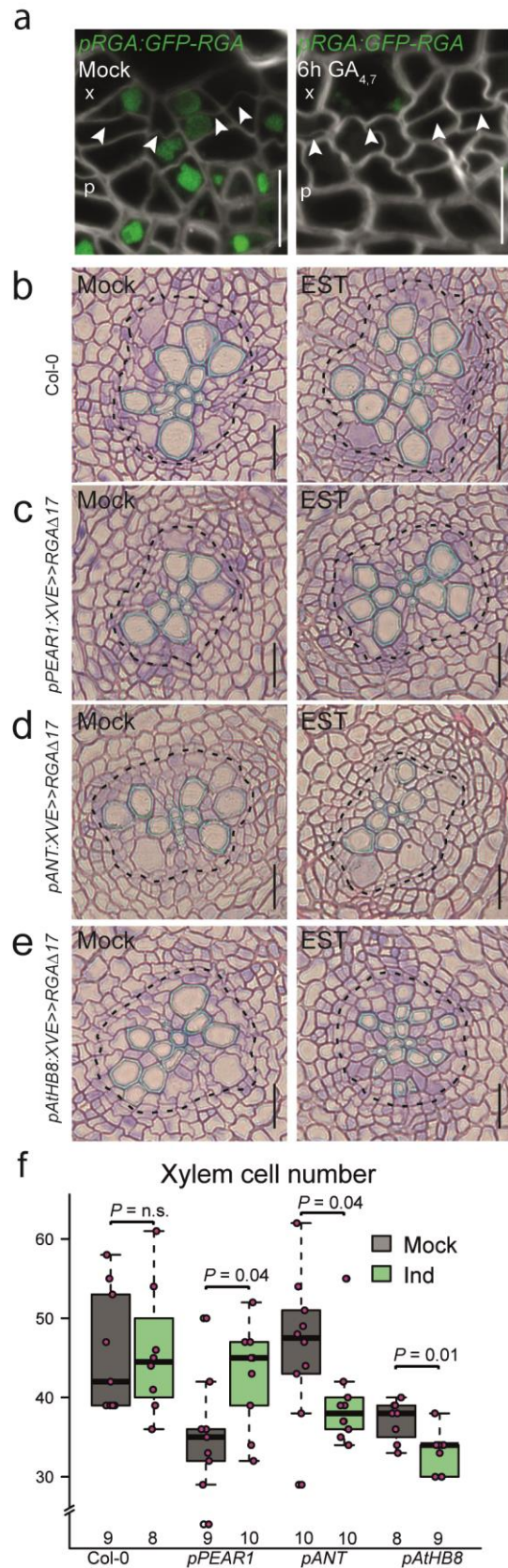


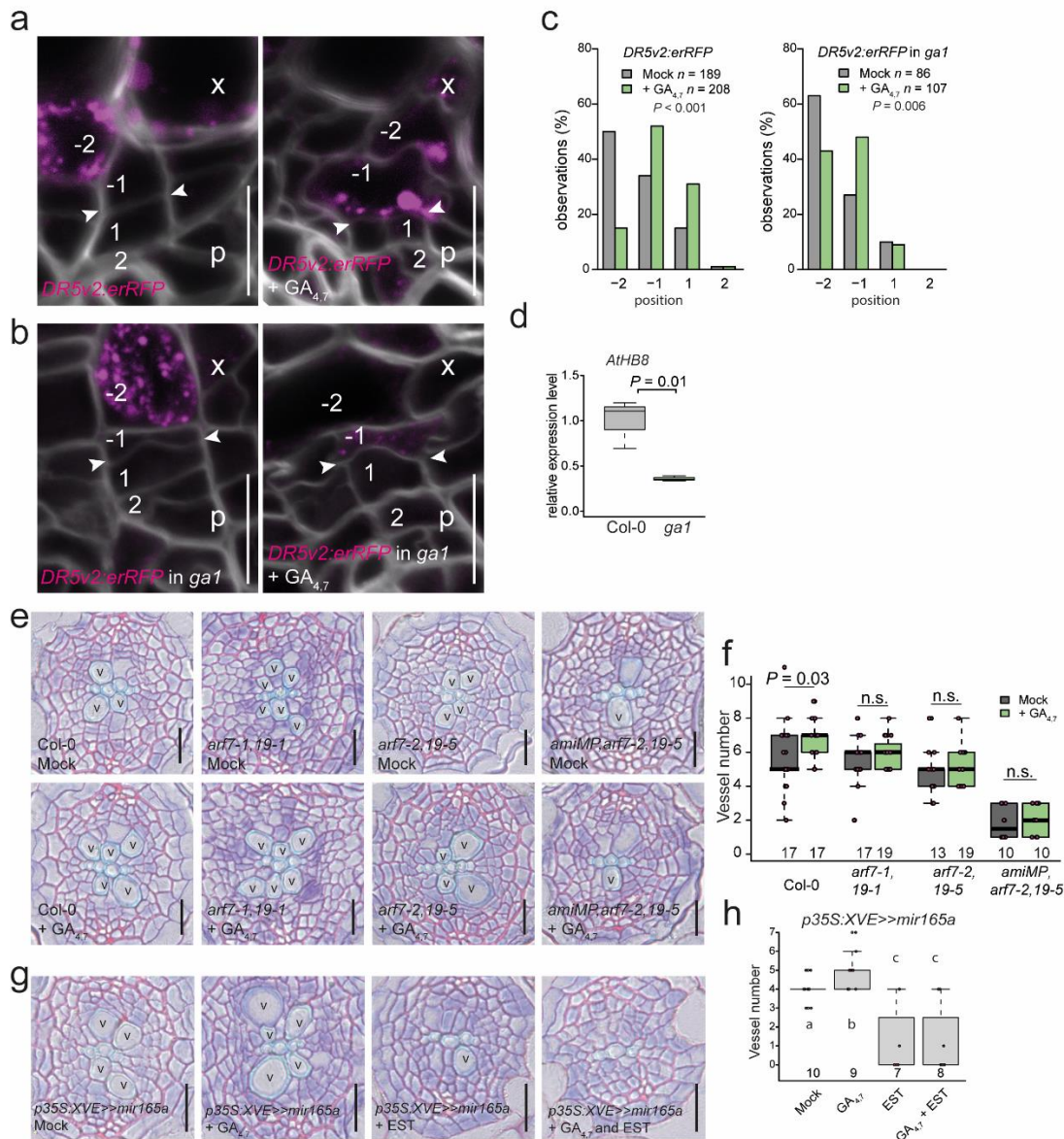
Figure 2. GA signalling on the xylem side of the cambium is required to promote secondary xylem formation. (a) Expression pattern of *pRGA::GFP-RGA* in the root cambium of 14-day old seedlings after a 6h mock or $GA_{4,7}$ treatment. White arrows indicate the most recent divisions. (b-e) Root cross-sections after a 6-day induction in 4-day old seedlings of Col-0 (b) or with mutated *RGAΔ17* expressed in the early phloem cell (*pPEAR1::XVE>>RGAΔ17*) (c), the stem cells (*pANT::XVE>>RGAΔ17*) (d), or the early xylem (*pATHB8::XVE>>RGAΔ17*) (e). Black dotted lines indicate the most recent divisions. (f) Quantification of the total xylem cell number (cells within the most recent cell divisions) in panels b-e. Scale bars are 10 μ m (a) or 20 μ m (b-e). Significant differences based on a two-tailed Wilcoxon-test are indicated. Numbers in f indicate number of samples. The boxes in the box and whisker plots show the median and the interquartile range, and the whiskers show the total range. Individual data points are plotted as purple dots. “p” = phloem, “x” = xylem. All experiments were repeated three times.

169 **GA regulates the width of the auxin response gradient to promote xylem formation**

170 Earlier clonal activation studies have shown that a local auxin maximum drives xylem formation and
171 promotes cambial cell divisions non-cell autonomously⁴. As GA's effect on xylem proliferation is the strongest
172 in the early xylem cells, where the local auxin signalling maximum is located, we investigated whether GA
173 could regulate the position of this maximum. Using a new RFP-based version of the auxin response reporter,
174 *DR5v2*³⁰ (see Methods), we observed expression on the xylem side of cambium (**Fig. 3a**), matching which cells
175 show the highest levels of auxin signalling in secondary tissues⁴. Recent stem cell divisions are identifiable by
176 the appearance of thin cell walls within the cambium (arrowheads in **Fig. 3a**). We marked the phloem-side
177 stem cell daughter as 1 and the xylem-side daughter as -1 (**Fig. 3a,b**). In wild type plants, *DR5v2* expression
178 often reaches the xylem-side stem cell daughter (-1) and even reached the cell in position -2, but it was rarely
179 seen in the phloem-side daughter. In *ga1*, a smaller proportion of stem cell daughters showed *DR5v2*
180 expression (expression in positions 1 or -1 was seen in 29% of *ga1* roots and 48% of Col-0 roots, **Fig. 3b**,
181 **Extended Data Fig. 2a**). A 24 h GA treatment was not sufficient to cause changes in *DR5v2* expression
182 (**Extended data Fig. 2b-d**). However, after 48 h, a higher proportion of the stem cell daughters expressed
183 *DR5v2* than in mock controls (57% in positions -1 and 1 in *ga1* and 83% in Col-0) (**Fig. 3a,b,c**). Altogether,
184 these GA manipulation studies show that GA regulates the position of the auxin signalling maximum within
185 cambium.

186 Since auxin drives xylem vessel formation⁴, this GA-induced broadened auxin response gradient could explain
187 how GA promotes vessel production (**Fig. 1a,b**). To the test this, we investigated whether auxin signalling is
188 required for the effect of GA on xylem production in the root cambium. Previously, we have shown that auxin
189 signalling in the *Arabidopsis* root cambium acts primarily via *MONOPTEROS (MP/ARF5)*, *ARF7* and *ARF19*⁴.
190 We therefore treated two different allelic *arf7,19* mutant combinations and the conditional triple mutant
191 *amiMP* (inducible artificial microRNA against *MP* in *arf7,19*⁴; see Methods) with GA. No significant changes
192 in the number of secondary xylem vessels were observed in any of the mutant combinations following GA
193 treatment (**Fig. 3e,f**), indicating that GA's effect on xylem production requires *ARF5/ARF7/ARF19*-mediated
194 auxin signalling.

195 The HOMEODOMAIN LEUCINE ZIPPER IIIs (HD-ZIP IIIs) act downstream of auxin signalling^{31,32} to promote
196 xylem identity in the root cambium⁴. A representative member of the family, *AtHB8*, is expressed specifically
197 in the early xylem cells⁴. Since *ga1* has a narrow auxin signalling maximum (**Fig. 3b; Extended Data Fig 2a**),
198 *AtHB8* expression is also reduced in the *ga1* mutant, as shown by qRT-PCR analysis (**Fig. 3d**). Inducible
199 overexpression of *mir165*, which targets the mRNAs of all five HD-ZIP IIIs for degradation³³, leads to the
200 inhibition of secondary xylem formation in the root cambium⁴. GA was unable to rescue this phenotype,
201 indicating that the HD-ZIP IIIs are required for GA-induced xylem production (**Fig. 3g,h**). Taken together, these
202 data show that GA's effect on xylem formation acts via auxin signalling and its downstream factors to define
203 xylem identity.



204

205 **Figure 3. Auxin is required for GA to affect xylem development.** Expression of *DR5v2:erRFP* in the root cambium after
 206 a 48 h GA treatment in 14-day old seedlings of wild type Col-0 (**a**) and *ga1* (**b**). White arrowheads indicate the most
 207 recent cell divisions. The numbers “-2”, “-1”, “1” and “2” indicate the relative position of the cells in respect to the most
 208 recent cell division, with negative values towards the xylem and positive towards the phloem. (**c**) Counts of the position
 209 in the cambium at which the *DR5v2:erRFP* gradient ends. Cellular positions on the x-axis correspond with the cellular
 210 position in panel **a** & **b**, and n refers to the total number of observations. (**d**) qRT-PCR analysis of the *AtHB8* expression
 211 level in wild type and *ga1* backgrounds. (**e**) Root cross-sections after a 6-day GA treatment in 4-day old seedlings of Col-
 212 0, *arf7,arf19*, and *amiMP,arf7,arf19*. (**f**) Quantification of the number of secondary xylem vessels in plants shown in
 213 panel **e**. (**g**) Root cross-sections after a 6-day induction and GA treatment in 4-day old seedlings of *p35S::XVE>>mir165a*
 214 seedlings. (**h**) Quantification of the number of secondary xylem vessels in plants shown in panel **g**. Chi-squared test in **c**;
 215 two-tailed t-test in **d,f**; two-way ANOVA with Tukey’s post hoc test in **h**. The boxes in the box and whisker plots show
 216 the median and the interquartile range, and the whiskers show the total range. Individual data points are plotted as
 217 purple dots. Numbers in **f** and **h** indicate number of samples. Letters indicate a significant difference, $P < 0.05$. “p”=
 218 phloem, “x” = xylem, “v” = secondary xylem vessels, n refers to the total number of observations. Scale bars are 10 μ m
 219 (**a,b**) or 20 μ m (**e,g**). All experiments were repeated three times.

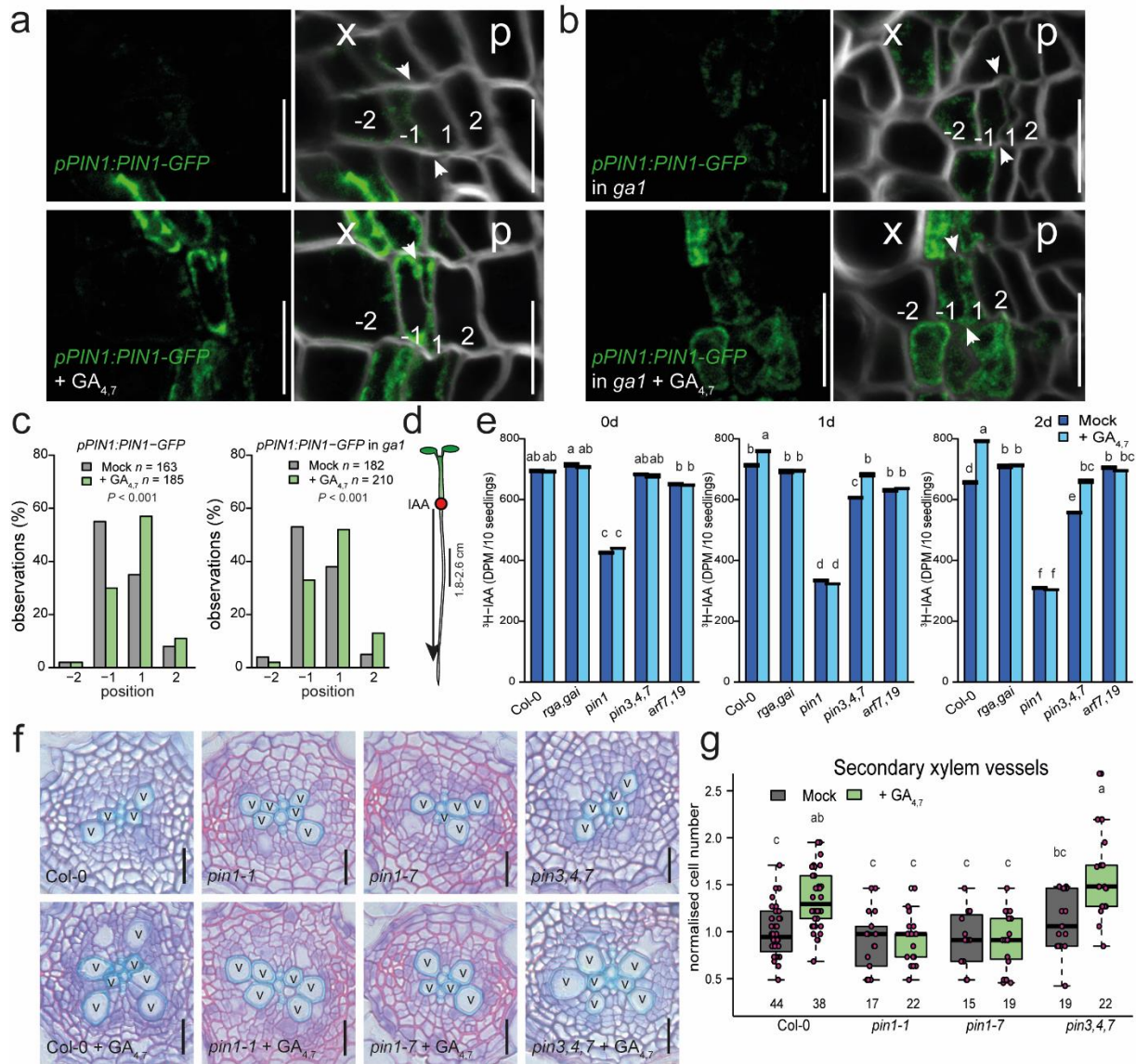
220 GA promotes long distance PAT via PIN1

221 The PIN auxin efflux carriers play a dominant role in determining how auxin accumulates in different tissues³⁴.
222 Since GA has previously been reported to regulate PIN levels in the root apical meristem^{22,35}, we investigated
223 whether GA also regulates auxin accumulation, and thus auxin signalling, through PIN activity in the vascular
224 cambium. Of the five plasma membrane-localized PINs (PIN1,2,3,4,7)³⁴, only PIN1 showed consistent
225 expression on the xylem side of the vascular cambium (**Extended Data Fig. 3a-e**). A detailed analysis revealed
226 that PIN1 has the highest expression in the xylem-side stem cell daughters (position -1), with weaker
227 expression in the neighbouring cells (positions -2 and 1). Following 24 h GA treatment, PIN1 expression
228 spreads towards the phloem to occupy both stem cell daughters (**Fig. 4a,c**), thus showing a shift in expression
229 similar to the auxin signalling marker *DR5v2*. However, *DR5v2* induction takes longer time (48 h) (**Fig. 3a-c**;
230 **Extended data Fig. 2b-d**). In the *ga1* mutant background, the PIN1 expression pattern is similar to the pattern
231 in wild type, but a similar shift in PIN1 expression was observed after GA treatment (**Fig. 4b,c**). Together,
232 these data show that GA promotes PIN1 expression in the stem cells and this is followed by expression of
233 *DR5v2*.

234 Previously, PIN1 has been proposed to act both via increased long distance PAT and via local redirection of
235 auxin fluxes^{11,13,34}. PIN1 has been shown to be basally localised in vascular cells^{11,13,36,37}. Similarly, in the root
236 cambial stem cells, we observed basal PIN1 localisation, which did not change after GA treatment (**Extended**
237 **Data Fig. 3f**). This suggests that GA does not redirect auxin fluxes within the cambium, implying that long
238 distance PAT might be affected. To test whether GA enhances long distance PAT, we performed a PAT assay.
239 6-day old seedlings were treated with GA_{4,7} for 1 h, after which seedlings were rinsed and then transferred
240 either directly to discontinuous media for auxin transport assay or replaced on MS media to grow for an extra
241 one or two days. For the PAT assay, tritium labelled indole-3-acetic acid (³H-IAA) was applied to the root-
242 shoot transition zone, and radioactivity was measured in either the upper part of the root (**Fig. 4d,e**) or the
243 root tip (**Extended Data Fig. 4a,b**). Increased ³H-IAA signals were observed in the upper part of GA-treated
244 wild type roots one day after GA application (**Fig. 4e**). As expected, in the DELLA double mutant *rga,gai*, in
245 which GA signalling is derepressed³⁸, the ³H-IAA signal did not increase upon GA treatment (**Fig. 4e**; **Extended**
246 **Data Fig. 4b**), thus demonstrating that GA's effect on PAT is caused by the canonical GA signalling pathway.
247 Similarly, *arf7,19* failed to respond to GA (**Fig. 4e**; **Extended Data Fig. 4b**), indicating that ARF7/19-mediated
248 auxin signalling is required for GA-induced PAT as well as for xylem formation (**Fig. 3e,f**).

249 As GA signalling is able to both enhance PAT and broaden PIN1 expression in the cambium, we postulated
250 that PIN1 might be required for GA's effect on PAT. The *pin1-7* loss-of-function mutant has a lower baseline
251 level of PAT, and *pin1* mutant roots did not show increased ³H-IAA transport upon GA treatment, similar to
252 *rga,gai* and *arf7,19* mutants (**Fig. 4e** and **Extended Data Fig. 4b**). However, GA treatment in the triple mutant
253 lacking three of the other plasma membrane localised PINs, *pin3,4,7*, did result in increased levels of ³H-IAA
254 in roots (**Fig. 4e** and **Extended Data Fig. 4b**), indicating that mainly PIN1 is required for GA's effect on long-
255 distance PAT.

256 In addition to PINs, two ATP Binding Cassette subfamily B (ABCB) auxin transporters, ABCB19 and ABCB21,
257 also contribute to maintenance of polar auxin transport streams in the vasculature^{39,40}. No change in *ABCB19*
258 expression was observed with GA treatment (**Extended Data Fig. 5a**). However, *ABCB21*, which is localised
259 almost exclusively to the pericycle⁴⁰, initially increased slightly with GA treatment and maintained over a 24
260 h period (**Extended Data Fig. 5a,b**). While rootward auxin transport was severely reduced in *abcb19*, mutants
261 still showed increased transport with GA treatment (**Extended Data Fig. 5c**). PAT in *abcb21* was only slightly
262 responsive to GA (**Extended Data Fig. 5c**). Together these results suggest that GA-enhanced long-distance
263 PAT requires ABCB19 function along with PIN1. Additionally, GA-upregulated ABCB21 likely increases
264 restriction of auxin to the central vasculature, where PIN1 provides directional flux toward the root tip in
265 addition to more localized auxin distributions within vascular cambium.



266

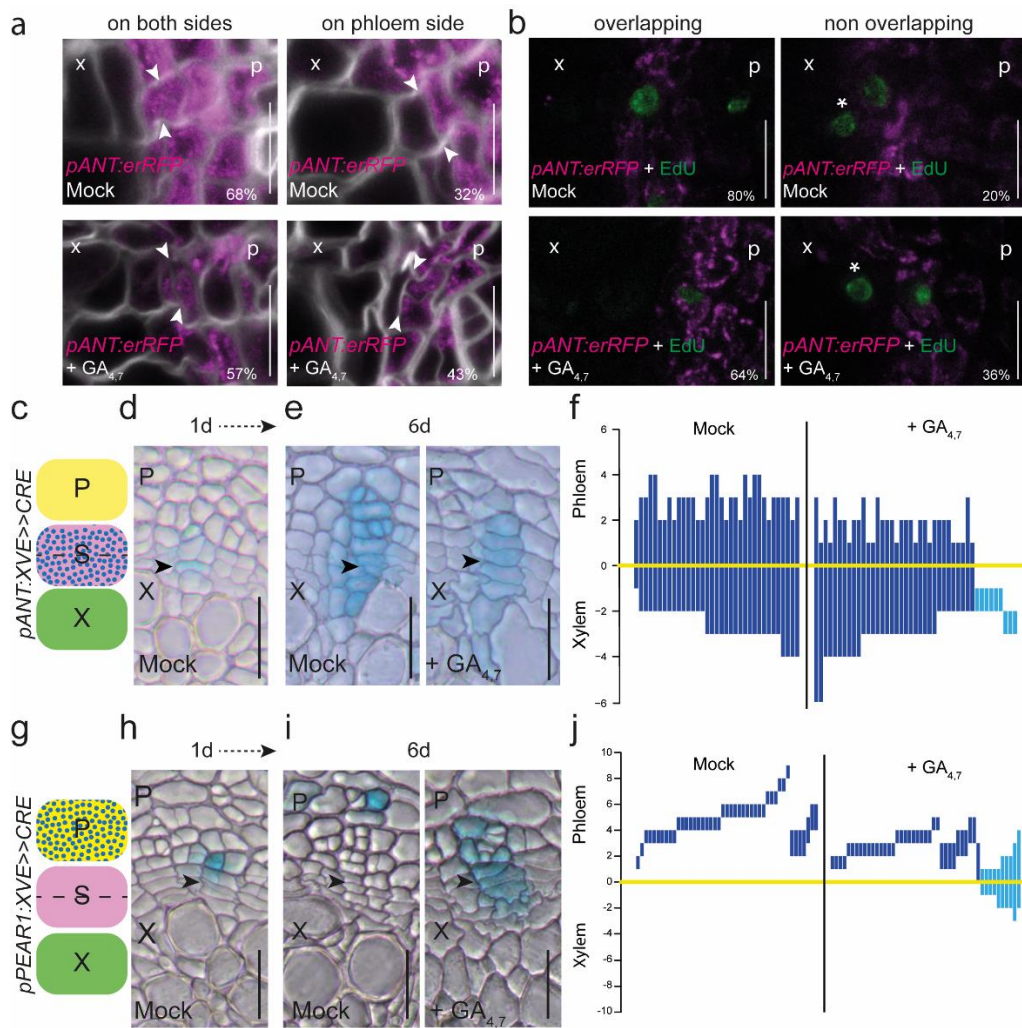
267 **Figure 4. GA promotes long-distance auxin transport in a PIN1-dependent manner.** Expression of *pPIN1:PIN1-GFP* in
 268 the root cambium after a 24 h GA treatment in 14-day old seedlings of wild type (a) and *ga1* (b). White arrowheads
 269 indicate the most recent cell divisions. The numbers “-2”, “-1”, “1” and “2” indicate the position of the cells relative to
 270 the most recent cell division, with negative values towards the xylem and positive towards the phloem. (c) Counts of
 271 the position in the cambium at which the *pPIN1:PIN1-GFP* gradient ends. Cellular positions on the x-axis correspond
 272 with the cellular positions in panels a & b, and n refers to the total number of observations. (d) A schematic explaining
 273 the setup of the PAT assay. The red circle indicates the position of 3H -IAA application, black arrow showing the direction
 274 of IAA movement. The black line indicates the area sampled to detect 3H -IAA. (e) 3H -IAA transport from the root-shoot
 275 transition zone to 1.8-2.6 cm from the root tip after a 1 h GA treatment in 6-day old Col-0 and mutant plants. After 0, 1,
 276 or 2 days, plants were treated with 3H -IAA for 3 h and then sampled. Data shown are means \pm SD (n = 3 independent
 277 pools of 10). (f) Root cross-sections after a 6-day GA treatment in 4-day old seedlings of Col-0 and various *pin*-mutants.
 278 (g) Quantification of the number of secondary xylem vessels in plants shown in panel f. Chi-squared test in c; two-way
 279 ANOVA with Tukey’s post hoc test in e and g. The boxes in the box and whisker plots show the median and the
 280 interquartile range, and the whiskers show the total range. Individual data points are plotted as purple dots. Numbers
 281 in g indicate number of samples. Letters indicate a significant difference, $P < 0.05$. Scale bars are 10 μ m (a,b) or 20 μ m
 282 (f). “p”= phloem, “x”= xylem, “v”= secondary xylem vessel. All experiments were repeated three times.

283 Since PIN1 has a central role in directional auxin flux along cambium, we next studied whether PIN1 is
284 required for GA to promote secondary xylem production. We first analysed the effect of GA treatment in two
285 allelic *pin1* mutants, *pin1-1* and *pin1-7*. GA treatment led to an increased number of secondary xylem vessels
286 in wild type but not in either of the *pin1* mutants (**Fig. 4f,g**). In contrast, the *pin3,4,7* mutant responded
287 similarly to wild type in terms of xylem production (**Fig. 4f,g**), indicating a non-redundant function for PIN1
288 in GA-induced xylem formation. Altogether, our data show that GA promotes broadening of PIN1 expression
289 in the cambium, which results in increased PAT along the hypocotyl and root. This leads to a broadening of
290 the high auxin signalling domain in cambium, thus promoting xylem production.

291 **GA treatment occasionally leads to stem cell respecification**

292 Next, we investigated how the GA-induced changes in the width of the auxin maximum alter stem cell fate
293 decisions, shifting from equal xylem and phloem distribution towards favouring xylem production (**Fig. 1f-i**).
294 First, we investigated the stem cell division dynamics using the stem cell marker *pANT:erRFP* together with
295 labelling dividing cells with 5-ethynyl-2'-deoxyuridine (EdU)⁴¹. *ANT* was typically expressed in both stem cell
296 daughters (mock: 68%; **Fig. 5a**) and to a lesser degree only in the phloem-side stem cell daughter (32%). After
297 two days of EdU tracing, the majority of the EdU-positive cells were in the *ANT* expression domain (mock:
298 80%; **Fig. 5b**). However, following a 2-day GA treatment, a larger proportion of *ANT* expression was restricted
299 to the phloem-side stem cell daughter (GA_{4,7}: 43%; **Fig. 5a**). In addition, significantly more EdU-positive cells
300 were outside the *ANT* expression domain towards the xylem (mock: 20%, GA: 36%; **Fig. 5b**). These data show
301 that GA treatment results in a higher proportion of xylem-side stem cell daughters losing stem cell identity
302 and obtaining xylem identity.

303 In order to follow the consequences of altered stem cell dynamics during long-term GA treatment, we carried
304 out a lineage tracing experiment where sectors marked with GUS expression were induced in the stem cells
305 using the *ANT* promoter (**Fig. 5c,d**)⁴. Under normal growth conditions, stem cell sectors spanned almost
306 equally towards both the xylem and the phloem (**Fig. 5e,f**), similar to the stem cell sectors generated
307 randomly within the cambium (**Fig. 1f,g,i**) and what we have shown earlier⁴. When seedlings are treated with
308 GA, the majority of the stem cell sectors spanned further towards xylem than phloem (**Fig. 5e,f**).
309 Unexpectedly, a subset of the *ANT*-sectors were pushed away from the cambium into the xylem (light blue
310 sectors in **Fig. 5f**, 21% of the GA sectors), indicating that, occasionally, both stem cell daughters lose their
311 identity and differentiate into xylem after GA application. This led us to hypothesise that when auxin
312 signalling spreads to both stem cell daughters causing them to differentiate into xylem, the adjacent phloem
313 identity cell respecifies as a stem cell. To test this, we performed a lineage tracing experiment with sectors
314 originating from a single early phloem cell using the promoter of phloem identity gene *PEAR1*²⁹ (**Fig. 5g,h**).
315 Under normal conditions, the active cambium pushes phloem identity cells away from the cambium while
316 they differentiate into phloem cells, leading to the formation of sectors deep in the phloem (**Fig. 5i,j**).
317 However, under GA-treated conditions, a subset of phloem lineage sectors is able to produce both xylem and
318 phloem (light blue sectors in **Fig. 5j**), 21% of the GA sectors), indicating that in these sectors the lineage
319 progenitor re-acquired stem cell identity. These data suggest that the original phloem identity cell
320 occasionally respecifies as a stem cell during GA treatment, thus supporting the respecification hypothesis.



321

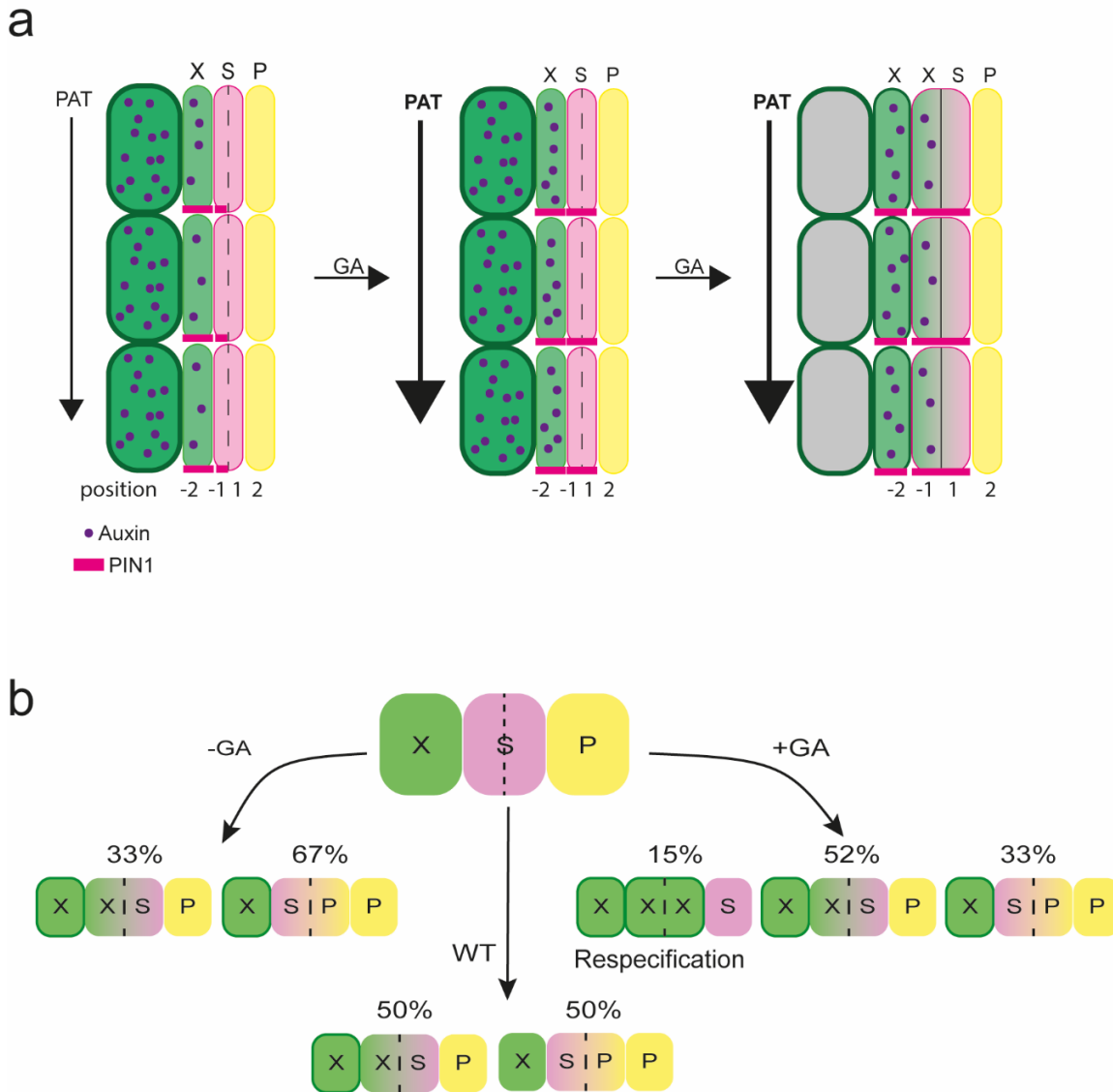
322 **Figure 5. GA promotes xylem formation by influencing cambial dynamics.** (a). Confocal root cross-sections of
 323 *pANT:erRFP* after a 48 h GA treatment in 14-day old seedlings. White arrowheads indicate the most recent cell divisions.
 324 A shift of expression to only the phloem-side stem cell daughter after GA treatment was significant, with a *P* value of
 325 0.0012 (chi-square test, $n_{\text{mock}}=407$, $n_{\text{GA}}=477$). (b) Confocal root cross-sections of *pANT:erRFP* (magenta) after 6 hours of
 326 EdU (green) incorporation and a 48 h GA treatment in 14-day old seedlings. White asterisks indicate EdU-positive cells
 327 that do not overlap with *pANT:erRFP* expression. The increase in EdU-positive nuclei not overlapping with *ANT*
 328 expression was significant, with a *P* value of 0.03 (chi-square test, $n_{\text{mock}}=100$, $n_{\text{GA}}=102$). The percentages in the corners
 329 of the subpanels represent the frequency of the observed phenotypes (a, b). (c) A schematic showing where *ANT* sectors
 330 originate from within the vascular cambium. (d) An example of a stem cell sector one day after induction in a 14-day old
 331 seedling. (e) Examples of stem cell sectors 6 days after induction in 14-day old seedlings grown on 2 μM GA_{4,7} or mock
 332 treatment. (f) GUS sectors (bars) plotted based on the position of the thinnest cell wall (yellow line). Note that the light
 333 blue bars highlight the sectors that are only present on the xylem side of the cambium (21% of the GA treated samples).
 334 (g) A schematic describing where the *PEAR1* sectors originate from within the vascular cambium. (h) An example of a
 335 phloem cell sector one day after induction in a 14-day old plant. (i) Examples of the phloem sectors 6 days after induction
 336 in 14-day old plants grown on 2 μM GA_{4,7} or mock treatment. (j) GUS sectors (bars) plotted based on the position of
 337 the thinnest cell wall (yellow line). Note that the light blue bars highlight the sectors that are able to produce both xylem
 338 and phloem (21% of the GA treated samples). “x”= xylem, “p”= phloem, “S”= stem cell. Black arrowheads indicate the
 339 most recent cell divisions. Percentages in a and b indicate frequency of the observed phenotype. Scale bars are 20 μm
 340 (d, e, h, i) or 10 μm (a, b). All experiments were repeated three times.

341 Discussion

342 We show that GA affects xylem proliferation in two ways: first, it increases the number of xylem cells
343 differentiating from the stem cells, and second, it promotes the expansion of secondary xylem vessels,
344 resembling the effect that GA has on other cell types in other tissues⁴². GA has the opposite effect on phloem
345 production: stem cells produce fewer phloem cells. However, despite the reduced total phloem cell number,
346 a higher proportion of conductive cells are produced. In turn, a GA biosynthesis mutant has a higher
347 proportion of parenchyma cells than conductive cells. Thus, even though GA levels have a clear impact on
348 phloem production, they have a smaller impact on the number of conductive phloem cells. This might be
349 important in ensuring phloem transport capacity regardless of GA status. Auxin promotes primary sieve
350 element differentiation in root tips⁴³. Since we show that GA increases auxin signalling in cambium and that
351 GA also promotes conductive phloem formation, we speculate that auxin is needed for the differentiation of
352 conductive phloem cell types also during secondary growth. Supporting this hypothesis, studies have shown
353 that GA and auxin together increase the production of phloem fibres^{44,45}.

354 We discovered that GA promotes PIN1-dependent and ABCB19/21-assisted PAT, which leads to elevated
355 auxin accumulation and signalling in the root cambium during the early stages of secondary development.
356 Previous studies have shown that the DELLAs and ARFs together regulate xylem production in the *Arabidopsis*
357 hypocotyl during flowering²¹. In poplar stems, GA promotes xylem production via *ARF7*, and this is associated
358 with transcriptional upregulation of *PIN1*^{46,47}. During leaf venation, PIN1 promotes auxin accumulation⁴⁸,
359 which leads to activation of ARFs⁴⁹. This in turn promotes *PIN1* expression, thus completing a feed-forward
360 loop⁵⁰. Our results show that GA induces PIN1 first, followed by upregulation of the ARF-regulated auxin
361 signalling reporter *DR5v2*. These results support a mechanism in which GA enters this feed-forward loop by
362 regulating the PIN1 expression pattern, at least during early secondary development in the *Arabidopsis* root.

363 Organizer cells in meristems position the stem cells to the adjacent cells. In the cambium, organizer cells are
364 defined by a local auxin signalling maximum and subsequent HD ZIP III expression that leads to cells acquiring
365 xylem identity and cell-autonomous inhibition of cell division⁴. In this study, we show that the position of the
366 maximum regulates the fate decisions of the stem cell daughters. In the presence of high GA and thus
367 elevated PAT, the xylem-side stem cell daughters accumulate high levels of auxin and therefore likely obtain
368 xylem/organizer identity. The phloem-side stem cell daughters retain stem cell identity (**Fig. 6a**).
369 Occasionally, both daughters accumulate high levels of auxin, leading both to obtain xylem/organizer
370 identity. This forces the neighbouring phloem identity cell to respecify as a stem cell (**Fig. 6b**). When GA levels
371 are low, both stem cell daughters have low auxin levels, thus making the xylem-side daughter maintain its
372 stem cell identity, since it is located adjacent to an existing auxin signalling maximum. Under these conditions,
373 the phloem-side daughter obtains phloem identity. It is unknown what positions the stem cells adjacent to
374 the auxin maximum. One possibility is that medium auxin levels within the auxin gradient promote stem cell
375 divisions. Supporting this idea, we previously observed an auxin signalling gradient along the cambium using
376 a sensitive auxin signalling reporter⁴. However, it is unclear how such a gradient could robustly position the
377 stem cells. Another possibility is that the auxin maximum initiates a mobile signal, which non-cell-
378 autonomously specifies stem cells in the adjacent position and promotes their division. However, the
379 existence of such a signal remains speculative.



380

381 **Figure 6. Models describing cambium dynamics** (a) Model showing what happens to PAT, PIN1 and auxin signalling
 382 upon GA treatment. Increased PAT induces PIN1 in the phloem-side stem cell daughter, and this leads to the widening
 383 of the auxin signalling maximum to the xylem-side stem cell daughter, which then gains xylem identity. The numbers
 384 “-2”, “-1”, “1” and “2” indicate the position of the cells relative to the most recent cell division, with negative values
 385 towards the xylem and positive towards the phloem. (b) Model explaining how the fate of the stem cell daughters is
 386 regulated by GA. In normal conditions, cambial stem cells produce an equal amount of xylem and phloem. With low
 387 GA levels, stem cell daughters preferentially gain phloem identity, while high GA levels lead to xylem identity, and in
 388 extreme cases the respecification of stem cells from phloem identity cells. X = xylem, S = stem cell (daughters), P =
 389 phloem.

390

391 Acknowledgements

392 We would like to thank Claus Schwechheimer, Enrico Scarpella and Laura Ragni for providing us published
 393 material; and Laura Ragni, Enrico Scarpella, Sedeer el-Showk, Hiroyuki Iida and Xixi Zhang for providing
 394 feedback on the manuscript. Confocal imaging was performed with help and using equipment of the Light
 395 microscopy Unit (LMU), University of Helsinki. Special thanks to Mikko Herpola and Miki Iida for helping with
 396 daily lab related tasks. This work was supported by the Academy of Finland (grants #316544, #346141),
 397 European Research Council (ERC-CoG CORKtheCAMBIA, agreement 819422), University of Helsinki (HiLIFE

398 fellowship and DPPS) and the US Department of Energy, Basic Energy Sciences, grant no. DE-FG02-06ER15804
399 to A.S.M. and M.K.J.

400

401 **Contributions**

402 A.P.M. conceived the project; A.P.M., R.M. and O.S. designed the experiments; R.M., O.S. and B.W.
403 performed the experiments, except M.K.J and A.S.M. designed and conducted the PAT experiment and
404 analysis of ABCBs; L.V. created the APL projections; A.S.G. provided preliminary data; M.L., L.Y., X.W. and R.S.
405 generated genetic material; A.P.M, R.M. and B.W. wrote the paper with input from all authors.

406

407 **Data availability**

408 All data supporting the findings of this article are available in this article and its supplementary information.
409 Source data are provided with this paper.

410

411 **Methods**

412 Gene accession numbers

413 The accession numbers of the genes in this study are: *CYCB1;1*, AT4G37490; *PEAR1*, AT2G37590; *ANT*,
414 AT4G37750; *AtHB8*, AT4G32880; *MIR165A*, AT1G01183; *MP*, AT1G19850; *ARF7*, AT5G20730; *ARF19*,
415 AT1G19220; *GA1*, AT4G02780 ; *RGA*, AT2G01570; *PIN1*, AT1G73590; *GAI*, AT1G14920; *PIN2*, AT5G57090;
416 *PIN3*, AT1G70940; *PIN4*, AT2G01420; *PIN7*, AT1G23080; *APL*, AT1G79430; *ABCB19*, AT3G28860; *ABCB21*,
417 AT3G62150.

418 Plant material and cloning

419 All entry clones, except p1R4z-DR5v2, were generated by PCR amplification of the desired sequence with the
420 primers listed in Table 1 followed by recombination into Multisite Gateway compatible pDONR entry vectors
421 (Table 2). The PCR fragment of *DR5v2*, which was amplified from genomic DNA isolated from *DR5v2:nlsGFP*³⁰,
422 was cloned into the *p1R4z-Bsal-ccdB-Bsal* entry vector via Golden Gate cloning to generate *p1R4z-DR5v2*.
423 The construction of *p1R4z-Bsal-ccdB-Bsal* and the Golden Gate cloning were done as previously described⁵¹.
424 The resulting entry vector, *p1R4z-DR5v2* was assembled together with *p221z-erRFP*⁵² and *p2R3z-nost*⁵² into
425 the destination vector *pHm43GW*⁵³ by a MultiSite Gateway LR reaction.

426 Multisite Gateway technology was used to combine entry clones carrying a promoter (1st box), gene of
427 interest or a tag (2nd box) and a tag or terminator (3rd box) with Gateway-compatible binary destination
428 vectors in a multisite Gateway LR clonase reaction. All of the expression vectors generated in this study are
429 listed in Table 3.

430 All of the expression vectors were dipped in the Col-0 background, and single insertion lines were screened
431 based on Mendelian segregation of the selection marker. Several single insertion lines were screened for
432 each construct to observe the most consistent phenotypes or expression patterns. A previously published
433 inducible miRNA against MP (*amiMP*)⁴ line was dipped into the *arf7-2,19-5* background due to silencing issues
434 in the earlier *arf7-1,19-1* background. Seeds published in this study, as well as the already published lines,
435 are listed in Supplementary Table 4. The following transgenic and mutant lines have been reported
436 elsewhere: *pHS:Dbox-CRE x 35S:lox-GUS*⁴, *p35S:XVE>>miR165a*⁴, *pANT:XVE-CRE x 35S:lox-GUS*⁴, *pPIN1:PIN1-*
437 *GFP*⁵⁴, *pPIN1:PIN1-GFP x ga1*²², *pPIN2:PIN2-GFP*⁵⁴, *pPIN3:PIN3-GFP*⁵⁵, *pPIN4:PIN4-GFP*⁵⁶, *pPIN7:PIN7-GFP*⁵⁶,
438 *pRGA:GFP-RGA*²⁷, *arf7-1,19-1*⁵⁷, *arf7-2,19-5*⁵⁸, *pin1-7* (SALK-047613)⁵⁹, *pin3,4,7*⁶⁰, *pin1-1*¹¹, *ga1* (SALK-
439 *109115*)²², *abcb19-101*⁶¹ and *abcb21-1*⁴⁰.

440 Plant growth and chemical treatments

441 Seeds were surface sterilised first with 20% chlorine and then with 70% ethanol, washed twice with H₂O and
442 then plated on a half-strength growth medium (½ GM, containing 0.5 × MS salt mixture with vitamins
443 (Duchefa), 1% sucrose, 0,5g/l MES pH 5.8 and 0.8% agar) and vernalized at 4 °C for 2 days. In the case of *ga1*
444 (SALK-109115), after sterilisation the seeds were soaked in 100 μM GA₃ for 5 days and covered at 4 °C. Before
445 plating, seeds were washed 5 times with H₂O. The age of the plants was measured from when the plates
446 were vertically positioned in the growth cabinet. The temperature in the cabinets was 22 °C and they had
447 long-day conditions (16h of light). In order to get seeds from *ga1* plants, plants growing in soil were sprayed
448 with 100 μM GA₃ twice per week until they had seeds.

449 10 mM and 100 mM stocks of GA_{4,7} (Duchefa) and GA₃ (Duchefa) were prepared in 100% EtoH and stored at
450 -20°C. A 10 mM stock of EdU, a thymidine analogue (Thermo Fisher), was made in DMSO and stored at -20 °C.
451 17-b-oestradiol (Sigma), a synthetic derivative of oestradiol, was prepared as a 20 mM stock solution in DMSO
452 and stored at -20 °C.

453 100 μM GA₃ was used for *ga1* seed germination and seed production. The working concentration for GA_{4,7}
454 was 2 μM. XVE-based gene induction was achieved by transferring plants onto plates containing 5 μM 17-b-
455 oestradiol or an equal volume of DMSO as a mock treatment. For EdU incorporation, plants were placed in
456 liquid ½GM containing 10 μM EdU for the time stated in each experiment.

457 GUS-staining, microtome sections and histology

458 The protocol was modified from Idänheimo et al.⁶². Samples were fixed with 90% acetone on ice for 30 min,
459 washed two times with a sodium phosphate buffer (0.05 M, pH 7.2) and then vacuum infiltrated with the
460 GUS-staining solution (0.05 M sodium phosphate buffer, pH 7.2; 1.5 mM ferrocyanide, 1.5 mM ferricyanide,
461 1 mM X-glucuronic acid, 0.1% Triton X-100). Samples were placed at 37 °C until the staining was at the desired
462 level (the required time varied between different lines).

463 After staining, the samples were fixed overnight in 1% glutaraldehyde, 4% formaldehyde, and 0.05 M sodium
464 phosphate pH 7.2. Fixed samples were dehydrated in an ethanol series (10%, 30%, 50%, 70%, 96%, 2x 100%),
465 with 30 minutes for each step, and then incubated for 1 h in a 1:1 solution of 100% ethanol and solution A
466 (Leica Histo-resin Embedding kit). After 2 h in solution A, samples were placed in plastic chambers and filled
467 with 14:1 mixture of solution A: hardener.

468 Sections of 5 or 10 μm were prepared on a Leica JUNG RM2055 microtome using a microtome knife (Leica
469 Disposable blades TC-65). The sections were imaged without staining or after staining with Safranin O (Sigma-
470 Aldrich) (1 min in 0,0125% solution, rinsed with water) or double staining with 0.05% Ruthenium Red (Sigma-
471 Aldrich) and Toluidine blue (Sigma Aldrich) (5 s in each, rinsed between stainings and afterwards with water).
472 Sections were mounted in water and visualised with a Leica 2500 Microscope.

473 Fluorescent marker analysis: vibratome sections and EdU detection

474 Using a protocol modified from Smetana et al.⁴, samples were vacuum infiltrated with 4% paraformaldehyde
475 solution (PFA, Sigma) in 1xPBS pH 7.2. After fixation, the samples were washed with PBS and embedded in
476 4% agarose. Embedded samples were cut with a vibratome into 200 μm sections for confocal analysis.
477 Agarose slices were placed into PBS with SR2200 (1:1000, Renaissance Chemicals) for cell wall staining. For
478 root tip visualizations, we fixed the samples with 4% PFA, cleared them with CLEARSEE, and stained the cell
479 walls with SR2200 as in Ursache et al.⁶³.

480 To visualise EdU-positive nuclei, EdU detection was performed on the agarose sections before cell wall
481 staining. The Click-iT EdU Alexa Fluor 488 Imaging Kit (Thermo Fisher) was used for detection with a modified
482 EdU detection mix⁴¹. Samples were incubated in the detection mix for 1 h on ice and then transferred into
483 PBS with SR2200 (1:1000).

484 Microscopy and image processing

485 Light microscopy images were taken with a Leica 2500 microscope (20x and 40x objectives). Fluorescent
486 markers were imaged with a Leica Stellaris 8 confocal microscope. Confocal images were obtained with Leica
487 Las AF software using PBS or water as the imaging medium. All confocal images with multiple channels were

488 imaged in sequential scan mode. Confocal settings may have varied between experiments but always stayed
489 the same for the experimental sample and the respective control. In order to better optimise the SR2200 cell
490 wall staining, the signal was sometimes adjusted during imaging and may thus vary between the sample and
491 control.

492 The Leica Stellaris 8 has a Tau-gating mode that makes it possible to separate GFP signals from background
493 signals. GFP markers were always imaged with this Tau-gating mode, gathering signals between 1.3-9 ns.

494 Image projections

495 For image projections (**Extended Data Fig. 1c-e**), each image was annotated by marking the centre of the
496 root and following the most recent cell division in each cell column in the cambium. The images have been
497 rotated so that the primary xylem axis is oriented in vertical position. Signal data from the image was sampled
498 from the centre point to the edges of the root and aligned to the most recent cell division in the cambial
499 zone. All images in the same treatment were then aligned with the annotated cambial line starting from the
500 centre to the edge. Images within each treatment can therefore be compared and analysed based on the
501 fluorescent signal distribution and intensity and the location/distance of cambium from the root centre.
502 Image wrapping was done using Python 3.8.10⁶⁴ and image ROI area extraction was done using several
503 different libraries, including OpenCV2⁶⁵, Pillow⁶⁶, Matplotlib v2.2.1⁶⁷ and NumPy⁶⁸. More detailed
504 documentation is available on Github (<https://github.com/LMIVainio/PolarUnwrap/find/main>).

505 Image analysis

506 Fiji/ImageJ was used for image analysis. When counting secondary xylem vessels, the primary xylem axis was
507 not included and only mature secondary vessels with light blue toluidine blue staining were counted. Cells
508 were counted with the cell counter tool. Xylem cells include all the cells inwards of the most recent
509 (=thinnest) cell division, so this also sometimes includes the stem cells and stem cell daughters (black line in
510 **Fig. 1A**). Phloem cells were counted as all the cells outwards from the most recent cell division until the
511 periderm border (clearly thicker continuous cell wall on the outskirts of the cross section: red line in **Fig.**
512 **1A**). In **Fig. 4f,g** (pin mutants), the data in the graph is combined from 4 separate experiments, so we
513 normalised the data from the experiments by giving the control (Col-0) the value of 1 and counting the other
514 values relative to that.

515 Analysis of the fluorescent markers was done with either Fiji/ImageJ or Leica LAS X lite. For *PIN1* and *DR5*, we
516 quantified the reach of the respective marker expression, meaning the position of the last cell in cambium
517 marker expression was seen. For the spread of *ANT*, we quantified the expression of the *ANT* marker in the
518 cambium, recording whether the marker was expressed on both sides of the most recent cell division or only
519 on the phloem side. Both of these quantifications were only done on cell lineages where the thinnest cell
520 wall was clearly recognisable. For the EdU pulse experiment, we quantified the number of EdU positive nuclei
521 that either overlapped with the *ANT* signal or were on its xylem side, and the number of those which are only
522 on the xylem side of *ANT* expression.

523 Auxin transport assays

524 6-day old seedlings on ½ MS agar plates were treated by applying a thin surface drench of 3 µM GA_{4,7}. After
525 1 hour, the solution was poured off and the seedlings were rinsed and gently blotted to remove excess
526 solution. The seedlings were then either transferred directly to a discontinuous filter paper system for
527 transport assays⁶⁹⁻⁷¹ or allowed to grow for an additional 1-2 days prior to the assays. For the auxin transport
528 assays, a 200 nL droplet of 10 µM ³H-IAA was placed at the root-shoot transition zone and the seedlings were
529 then incubated under low yellow light. After 3 hours, 8 mm segments were collected from two different
530 positions along the root: apex-0.8 cm (=root tip) and 1.8-2.6 cm (=upper part). ³H-IAA was measured by liquid
531 scintillation counting. The 1.8-2.6 cm segments contained lateral root primordia and emerged lateral roots.
532 Data shown are means ± SD (3 independent pools of 10 seedlings).

533 qRT-PCR

534 RNA was collected from 2 cm long pieces starting just below the hypocotyl of 10-day old roots where lateral
535 roots had been removed. RNA was isolated using the GeneJET Plant RNA Purification Mini kit (Thermo Fisher)
536 and treated with DNase. cDNA was synthesised from 100 ng of RNA using Maxima H Minus reverse
537 transcriptase (Thermo Fisher) and oligodT primers (Thermo Fisher). The PCR reaction was done on a Bio-Rad
538 CFX384 cyler using EvaGreen qPCR mix (Solis Biodyne) and the following program: 10 min at 95 °C, 50 cycles
539 (10 s at 95 °C, 10 s at 60 °C, 30 s in 72 °C). All of the primers used in qRT-PCR are listed in Table 1. The results
540 were normalised, following earlier published methods^{72,73}, to the reference genes *ACT2*, *UBQ10* and *TIP41*.
541 Three biological replicates were used for each line and treatment, as well as three technical replicates.

542 For ABCB21 expression, 7d seedlings were surface drenched with MS solution containing solvent control, 1
543 μ M, or 10 μ M GA for 15 mins. Solutions were decanted then plates returned upright in light for 24h. Total
544 RNA was isolated with TRIzol (Thermo Fisher) followed by lithium chloride precipitation. 1.5 μ g total RNA was
545 reverse transcribed with Superscript III (Thermo Fisher). PCR reactions were performed on a Bio-Rad CFX96
546 cyler using SYBR Green master mix (Applied Biosystems) and the following program: 3 m at 95°C, 45 cycles
547 (15s at 95°C, 1 min at 60°C). Expression was normalized to the reference genes ACT2 and PP2A. Primers used
548 were from Jenness et al., (2019)⁴⁰.

549 ANT EdU pulse experiment

550 A short 6 h pulse of 10 μ M EdU in liquid $\frac{1}{2}$ GM was used, after which the EdU was removed by washing twice
551 for 15 min with liquid $\frac{1}{2}$ GM. Washed plants were transferred into 2 μ M GA_{4,7} or EtOH plates and allowed to
552 grow for 2 days. After this, they were fixed for agarose sections and confocal analysis.

553 Lineage tracing

554 All lineage tracing experiments were performed in 16-day old plants. For the *pHSdboxCRE* plants, plates were
555 placed at 37°C for 14 or 17 minutes. They were then immediately cooled at 4 °C for 15 minutes⁴. The plants
556 were then transferred to 2 μ M GA_{4,7} or EtOH plates for 6 days. For the oestradiol-inducible lineage tracing
557 lines, plants were incubated in 5 μ M EST in liquid $\frac{1}{2}$ GM for two hours (*pPEAR1:XVE>>CRE*) or 30 min
558 (*pANT:XVE>>CRE*), washed 3x 15 min and then transferred to 2 μ M GA_{4,7} or EtOH plates for 6 days. For the
559 *pHSdboxCRE* experiments, we considered for the analysis only the sectors that proliferated.

560 General methodology and statistical analysis

561 The number of individual plants, cross sections or clones analysed is displayed as the n in figures or figure
562 legends. The fraction in the corner of some images indicates the frequency of the observation. All statistical
563 analyses were performed using R version 4.1.2 (<http://www.r-project.org/>).

564 All measurements were taken from distinct samples and the same sample was not measured repeatedly.

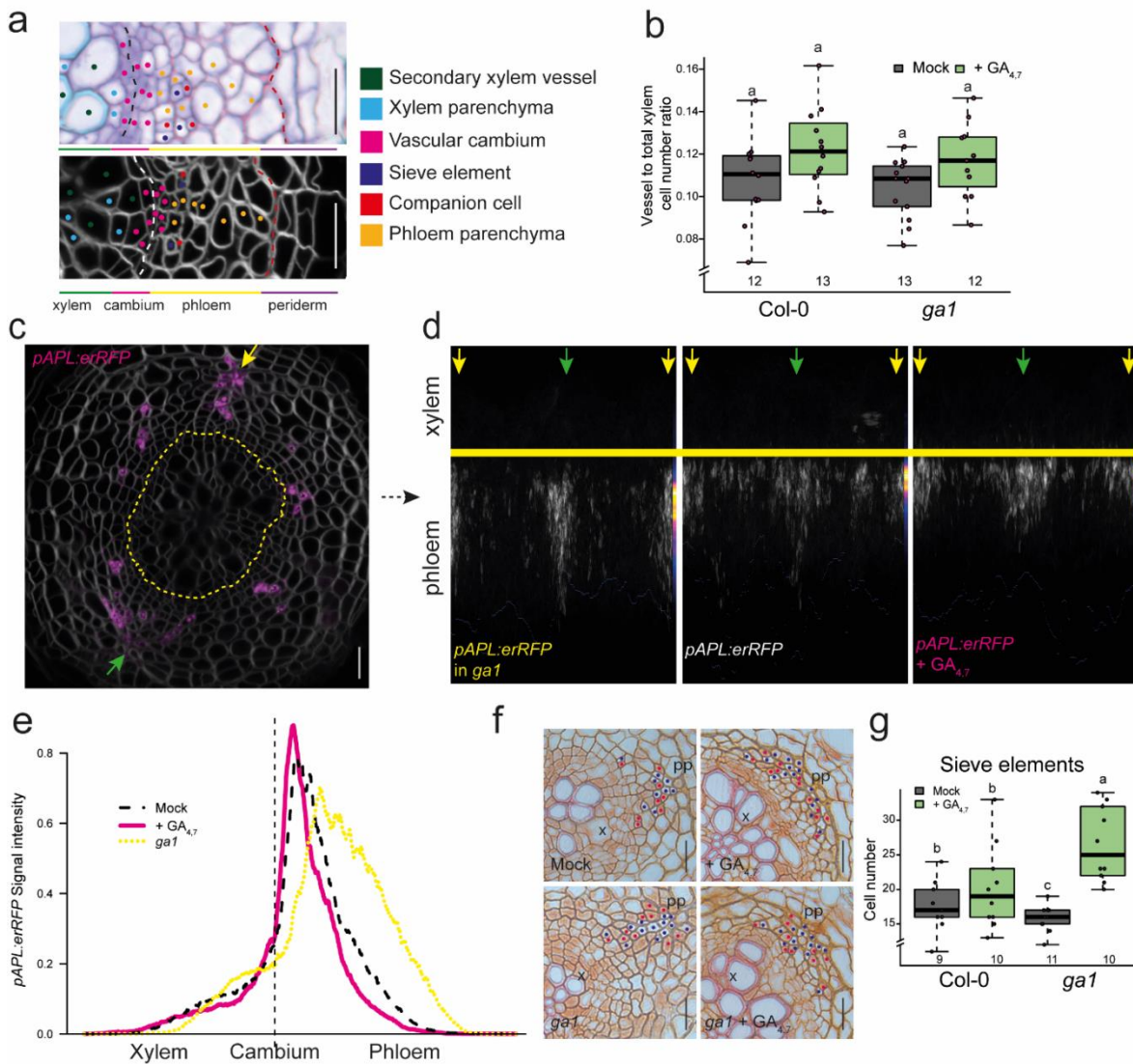
565 Before comparing means, the normality of the data was confirmed with the Shapiro-Wilk test. When doing
566 pairwise comparisons, normally distributed data were analysed with a 2-tailed t-test and other data with a
567 2-tailed nonparametric Wilcoxon test. When comparing multiple means with each other, a two-way ANOVA
568 with Tukey post hoc was performed. Categorical data were analysed with a chi-squared test.

569 In all of the box plots, the centre line represents the median, and the upper and lower box limits indicate the
570 75th and 25th percentiles, respectively. Whiskers show the maximum and minimum values, and outliers are
571 shown as circles. Filled circles represent individual data points. In violin plots, the white dot shows the median
572 and the thick line the interquartile range. The thinner line represents the rest of the distribution. Each side
573 of the line is a kernel density estimation that shows the distribution shape of the data. Filled circles represent
574 individual data points.

575 Softwares used

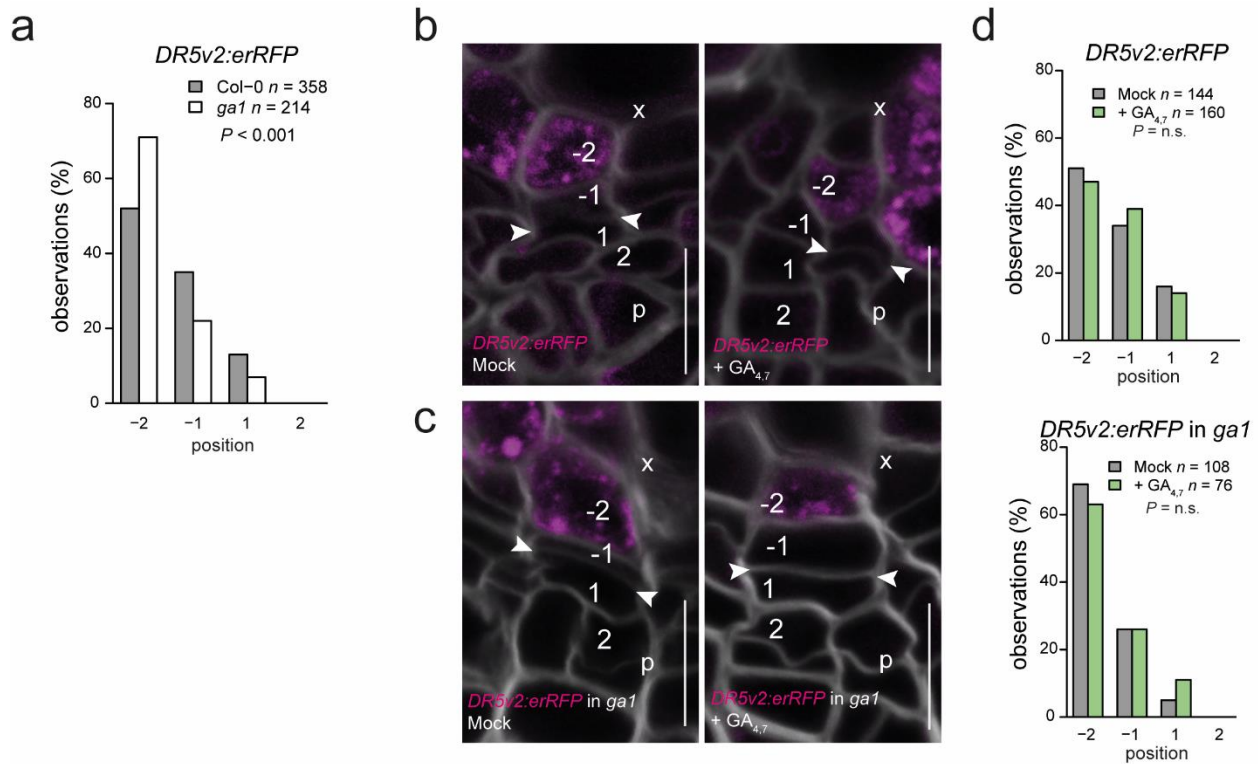
576 Leica LAS x, Leica LAS x lite, Bio-Rad CFX Manager, Fiji 1.53, R 4.1.2, R-studio, Adobe Illustrator, Python
577 3.8.10, MS Office: Excel, Word

578 **Extended Data Figures**



579

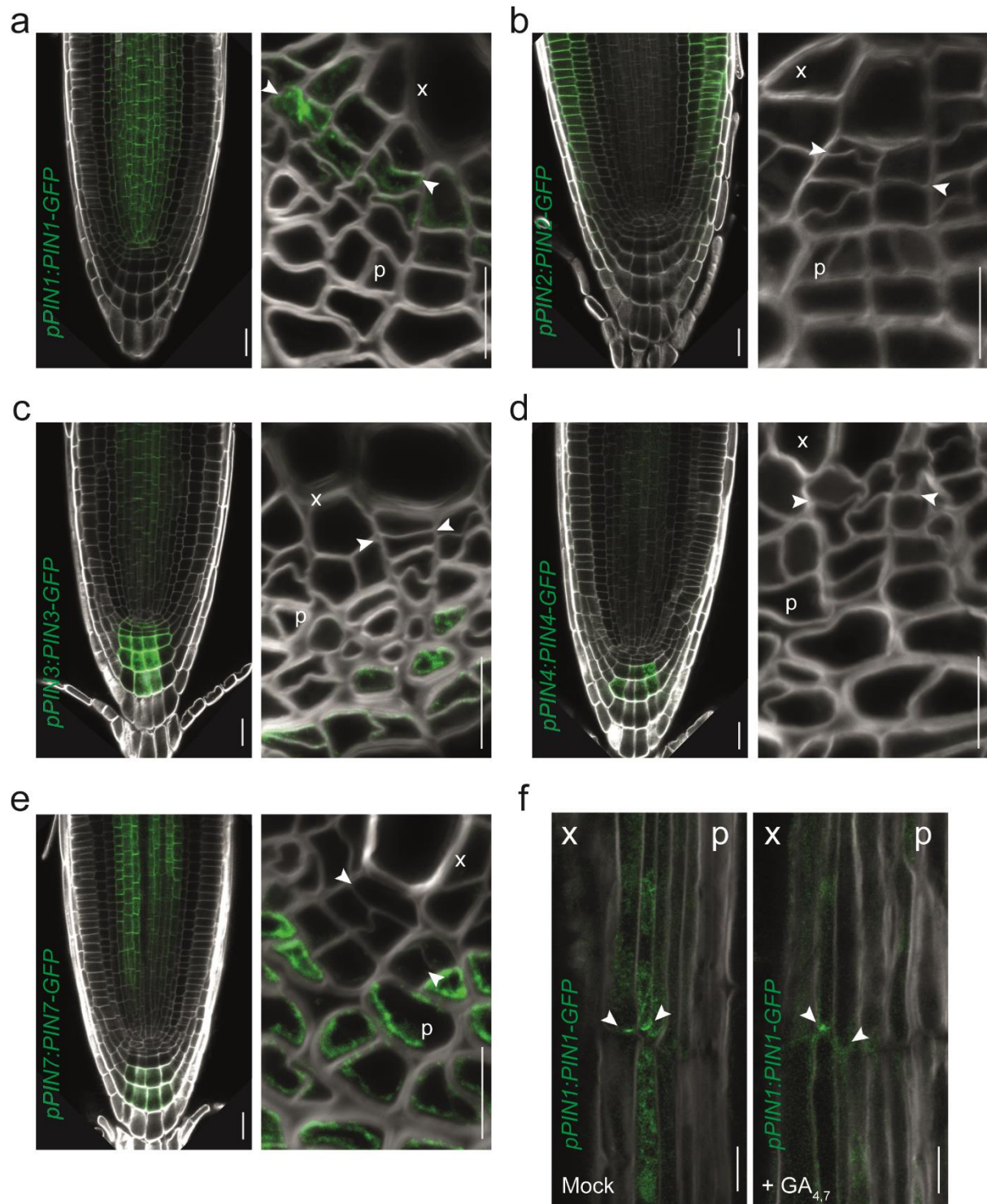
580 **Extended Data Figure 1. Characterisation of secondary tissues after GA treatment** (a) Schematic describing
 581 secondary growth tissue and cell types in plastic and agarose sections of 14-day old roots. Black dotted lines
 582 indicate the most recent cell divisions. Red dotted lines mark the border between the phloem parenchyma
 583 cells and the periderm. (b) The ratio of secondary xylem vessels to total xylem cell number. (c) An example
 584 of *pAPL:erRFP* expression in 14-day old roots. The dashed yellow line marks the most recent cell divisions. (d)
 585 Projections of *pAPL:erRFP* roots of 4-day old plants grown for 10 days on mock or 2 μ M GA_{4,7} plates or crossed
 586 into *ga1*. Each picture is combined from ~15 pictures with the phloem poles and thinnest cell walls aligned.
 587 The cambium is marked by a yellow line. Yellow and green arrows point to the primary phloem poles. Heat
 588 maps on the side show where the expression accumulates. (e) Graph showing *APL* expression relative to the
 589 cambium position. (f) Safranin-stained cross-sections of Col-0 and *ga1* 4-day old plants treated for 10 days
 590 with 2 μ M GA_{4,7} or mock. Safranin O does not stain sieve elements (blue dots), thus they stay white and are
 591 easy to distinguish. Companion cells are marked with red dots. (g) Quantification of the number of sieve
 592 elements in safranin-stained cross-sections. "x" = xylem, "pp" = primary phloem pole. Two-way ANOVA with
 593 Tukey's post hoc test in **b, g**. The boxes in the box and whisker plots show the median and interquartile range,
 594 and the whiskers show the total range. Individual data points are plotted as purple dots. Letters indicate
 595 significant differences, with $P < 0.05$. Scale bars are and 20 μ m (**a,c,f**). All experiments were repeated three
 596 times.



597

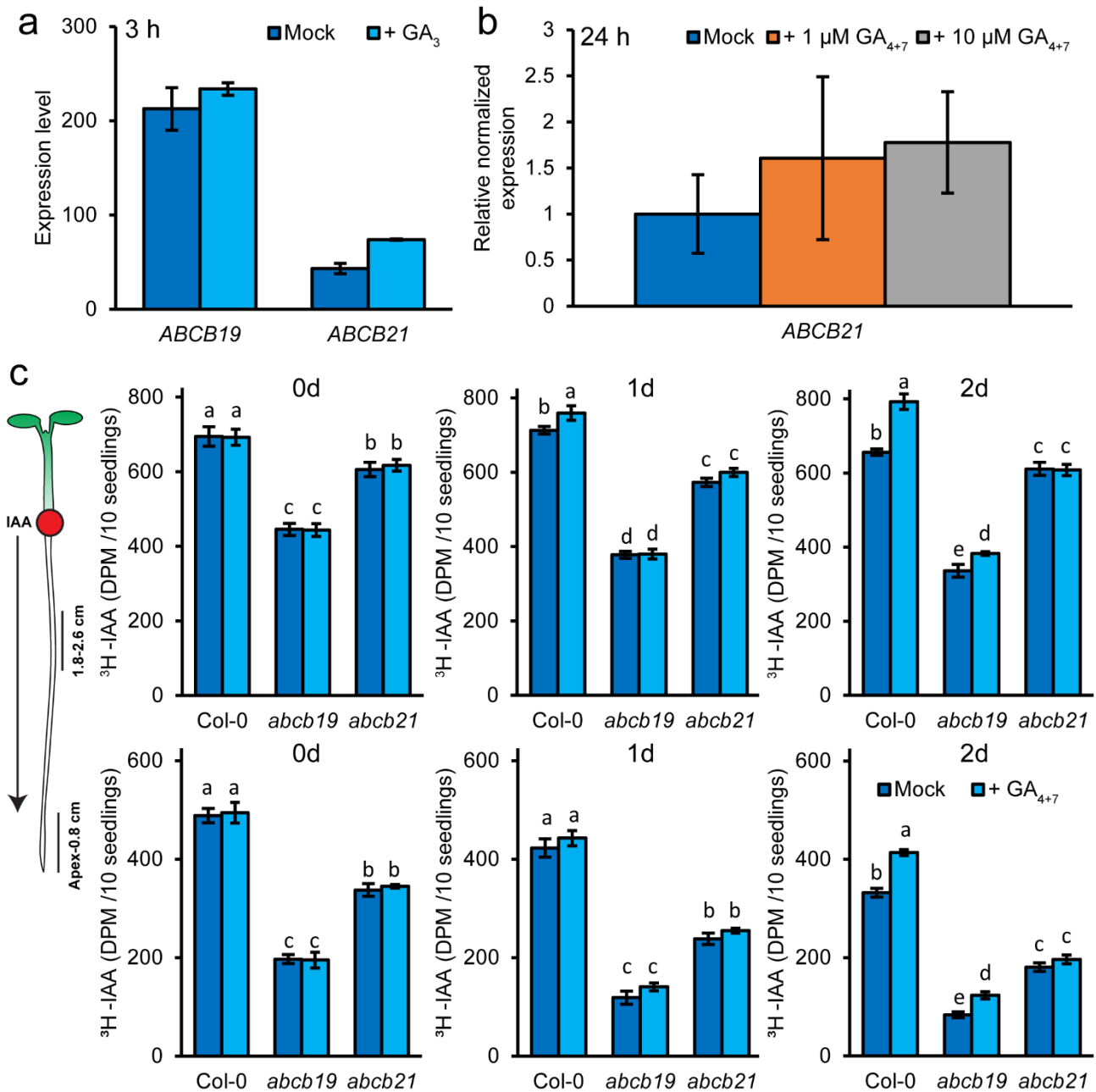
598 **Extended Data Figure 2. A 24h GA treatment is not sufficient to affect auxin signalling in the cambium.** (a)
 599 Graph comparing the extent of *DR5* in mock-treated 16-day old seedlings of Col-0 and *ga1*. Data is combined
 600 from 3 separate repeats. (b,c) *DR5v2:erRFP* expression after a 24 h treatment with 2 μ M *GA*_{4,7} in 14-day old
 601 seedlings of Col-0 (b) and *ga1* (c). The numbers “-2”, “-1”, “1” and “2” indicate the position of the cells relative
 602 to the most recent cell division, with negative values towards the xylem and positive towards the phloem.
 603 (d) Count of the position in the cambium at which the *DR5v2:erRFP* gradient ends. Cellular positions on the
 604 x-axis correspond with the cellular positions in panels b & c. “p”= phloem, “x”= xylem, arrows indicate the
 605 most recent cell divisions. Chi-squared test in a & d. n refers to the total number of observations. All
 606 experiments were repeated three times.

607



608

609 **Extended Data Figure 3. PIN expression patterns in the root tips and vascular cambium.** (a) pPIN1:PIN1-GFP
610 (b) pPIN2:PIN2-GFP (c) pPIN3:PIN3-GFP (d) pPIN4:PIN4-GFP (e) pPIN7:PIN7-GFP expression in 7-day old root
611 tips and 14-day old vascular cambium (a-e). Root tips act as positive controls to show that the marker lines
612 have the expected expression pattern in well-studied parts of the root. (f) Longitudinal sections showing
613 pPIN1:PIN1-GFP following a 24 h GA or mock treatment in 14-day old plants. “x”= xylem, “p”= phloem. Scale
614 bars are 20 μ m in the root tips and 10 μ m in the cambium and longitudinal sections. All experiments were
615 repeated three times.



624

625 **Extended Data Figure 5. PAT in *abcb* mutants.** (a) *ABCB19* and *ABCB21* expression 3 h after treatment with
626 1 μM GA₃ from the Arabidopsis eFP Browser⁷⁴. (b) Quantitative real-time PCR showing *ABCB21* expression
627 24 h after treatment with 1 or 10 μM GA₄₊₇. Data shown are means ± SD (n = 3 biological replicates, 2
628 technical replicates). (c) ³H-IAA transport in *abcb19* and *abcb21* mutant backgrounds from the root-shoot
629 transition zone to 1.8-2.6 mm from the root tips (upper panels) or to the root tips (lower panels) after 1h
630 GA treatment (in 6-days old plants). After 0, 1, or 2 days plants were treated with ³H-IAA for 3h and then
631 sampled. ³H-IAA transport in Col-0 shown is derived from the same set of experiments shown in Figure 4
632 and Extended Data Figure 4. Figure Data shown are means ± SD (n = 3 independent pools of 10). two-way
633 ANOVA with Tukey's post hoc test in c. Letters indicate significant difference in p < 0.05.

634

635 **References**

- 636 1 Chaffey, N., Cholewa, E., Regan, S. & Sundberg, B. Secondary xylem development in Arabidopsis: a
637 model for wood formation. *Physiol Plant* **114**, 594-600, doi:10.1034/j.1399-3054.2002.1140413.x
638 (2002).
- 639 2 Nieminen, K., Blomster, T., Helariutta, Y. & Mahonen, A. P. Vascular Cambium Development.
640 *Arabidopsis Book* **13**, e0177, doi:10.1199/tab.0177 (2015).
- 641 3 Evert, R. *Esau's Plant Anatomy, Meristems, Cells, and Tissues of the Plant Body: their Structure,*
642 *Function, and Development. 3rd edn.,* Vol. 3rd Edition (New Jersey: John Wiley & Sons, Inc, 2006).
- 643 4 Smetana, O. *et al.* High levels of auxin signalling define the stem-cell organizer of the vascular
644 cambium. *Nature* **565**, 485-489, doi:10.1038/s41586-018-0837-0 (2019).
- 645 5 Shi, D., Lebovka, I., Lopez-Salmeron, V., Sanchez, P. & Greb, T. Bifacial cambium stem cells generate
646 xylem and phloem during radial plant growth. *Development* **146**, doi:10.1242/dev.171355 (2019).
- 647 6 Bossinger, G. & Spokevicius, A. V. Sector analysis reveals patterns of cambium differentiation in
648 poplar stems. *J Exp Bot* **69**, 4339-4348, doi:10.1093/jxb/ery230 (2018).
- 649 7 Uggla, C., Moritz, T., Sandberg, G. & Sundberg, B. Auxin as a positional signal in pattern formation in
650 plants. *P Natl Acad Sci USA* **93**, 9282-9286, doi:DOI 10.1073/pnas.93.17.9282 (1996).
- 651 8 Bagdassarian, K. S., Brown, C. M., Jones, E. T. & Etchells, P. Connections in the cambium, receptors
652 in the ring. *Curr Opin Plant Biol* **57**, 96-103, doi:10.1016/j.pbi.2020.07.001 (2020).
- 653 9 Brackmann, K. *et al.* Spatial specificity of auxin responses coordinates wood formation. *Nat*
654 *Commun* **9**, 875, doi:10.1038/s41467-018-03256-2 (2018).
- 655 10 Przemeck, G. K., Mattsson, J., Hardtke, C. S., Sung, Z. R. & Berleth, T. Studies on the role of the
656 Arabidopsis gene MONOPTEROS in vascular development and plant cell axialization. *Planta* **200**,
657 229-237, doi:10.1007/BF00208313 (1996).
- 658 11 Galweiler, L. *et al.* Regulation of polar auxin transport by AtPIN1 in Arabidopsis vascular tissue.
659 *Science* **282**, 2226-2230, doi:10.1126/science.282.5397.2226 (1998).
- 660 12 Verna, C., Ravichandran, S. J., Sawchuk, M. G., Linh, N. M. & Scarpella, E. Coordination of tissue cell
661 polarity by auxin transport and signaling. *Elife* **8**, doi:10.7554/eLife.51061 (2019).
- 662 13 Bishopp, A. *et al.* A mutually inhibitory interaction between auxin and cytokinin specifies vascular
663 pattern in roots. *Curr Biol* **21**, 917-926, doi:10.1016/j.cub.2011.04.017 (2011).
- 664 14 Rodriguez-Villalon, A. *et al.* Molecular genetic framework for protophloem formation. *Proc Natl*
665 *Acad Sci U S A* **111**, 11551-11556, doi:10.1073/pnas.1407337111 (2014).
- 666 15 Kondo, Y., Fujita, T., Sugiyama, M. & Fukuda, H. A novel system for xylem cell differentiation in
667 Arabidopsis thaliana. *Mol Plant*, doi:10.1093/mp/ssu122 (2014).
- 668 16 Mazur, E., Benkova, E. & Friml, J. Vascular cambium regeneration and vessel formation in wounded
669 inflorescence stems of Arabidopsis. *Sci Rep* **6**, 33754, doi:10.1038/srep33754 (2016).
- 670 17 Ragni, L. *et al.* Mobile gibberellin directly stimulates Arabidopsis hypocotyl xylem expansion. *Plant*
671 *Cell* **23**, 1322-1336, doi:10.1105/tpc.111.084020 (2011).
- 672 18 Mauriat, M. & Moritz, T. Analyses of GA20ox- and GID1-over-expressing aspen suggest that
673 gibberellins play two distinct roles in wood formation. *Plant Journal* **58**, 989-1003,
674 doi:10.1111/j.1365-313X.2009.03836.x (2009).
- 675 19 Israelsson, M., Sundberg, B. & Moritz, T. Tissue-specific localization of gibberellins and expression
676 of gibberellin-biosynthetic and signaling genes in wood-forming tissues in aspen. *Plant J* **44**, 494-
677 504, doi:10.1111/j.1365-313X.2005.02547.x (2005).
- 678 20 Immanen, J. *et al.* Cytokinin and Auxin Display Distinct but Interconnected Distribution and
679 Signaling Profiles to Stimulate Cambial Activity. *Curr Biol* **26**, 1990-1997,
680 doi:10.1016/j.cub.2016.05.053 (2016).
- 681 21 Ben-Targem, M., Ripper, D., Bayer, M. & Ragni, L. Auxin and gibberellin signaling cross-talk
682 promotes hypocotyl xylem expansion and cambium homeostasis. *J Exp Bot* **72**, 3647-3660,
683 doi:10.1093/jxb/erab089 (2021).

- 684 22 Willige, B. C., Isono, E., Richter, R., Zourelidou, M. & Schwechheimer, C. Gibberellin Regulates PIN-
685 FORMED Abundance and Is Required for Auxin Transport-Dependent Growth and Development in
686 Arabidopsis thaliana. *Plant Cell* **23**, 2184-2195, doi:10.1105/tpc.111.086355 (2011).
- 687 23 Sun, T. P. & Kamiya, Y. The Arabidopsis GA1 locus encodes the cyclase ent-kaurene synthetase A of
688 gibberellin biosynthesis. *Plant Cell* **6**, 1509-1518, doi:10.1105/tpc.6.10.1509 (1994).
- 689 24 Bonke, M., Thitamadee, S., Mahonen, A. P., Hauser, M. T. & Helariutta, Y. APL regulates vascular
690 tissue identity in Arabidopsis. *Nature* **426**, 181-186, doi:10.1038/nature02100 (2003).
- 691 25 Bond, J., Donaldson, L., Hill, S. & Hitchcock, K. Safranin fluorescent staining of wood cell walls.
692 *Biotech Histochem* **83**, 161-171, doi:10.1080/10520290802373354 (2008).
- 693 26 Daviere, J. M. & Achard, P. Gibberellin signaling in plants. *Development* **140**, 1147-1151,
694 doi:10.1242/dev.087650 (2013).
- 695 27 Silverstone, A. L. *et al.* Repressing a repressor: gibberellin-induced rapid reduction of the RGA
696 protein in Arabidopsis. *Plant Cell* **13**, 1555-1566, doi:10.1105/tpc.010047 (2001).
- 697 28 Dill, A., Jung, H. S. & Sun, T. P. The DELLA motif is essential for gibberellin-induced degradation of
698 RGA. *P Natl Acad Sci USA* **98**, 14162-14167, doi:DOI 10.1073/pnas.251534098 (2001).
- 699 29 Miyashima, S. *et al.* Mobile PEAR transcription factors integrate positional cues to prime cambial
700 growth. *Nature* **565**, 490-494, doi:10.1038/s41586-018-0839-y (2019).
- 701 30 Liao, C. Y. *et al.* Reporters for sensitive and quantitative measurement of auxin response. *Nat*
702 *Methods* **12**, 207-210, 202 p following 210, doi:10.1038/nmeth.3279 (2015).
- 703 31 Donner, T. J., Sherr, I. & Scarpella, E. Regulation of preprocambial cell state acquisition by auxin
704 signaling in Arabidopsis leaves. *Development* **136**, 3235-3246, doi:10.1242/dev.037028 (2009).
- 705 32 Ursache, R. *et al.* Tryptophan-dependent auxin biosynthesis is required for HD-ZIP III-mediated
706 xylem patterning. *Development* **141**, 1250-1259, doi:10.1242/dev.103473 (2014).
- 707 33 Mallory, A. C. *et al.* MicroRNA control of PHABULOSA in leaf development: importance of pairing to
708 the microRNA 5' region. *EMBO J* **23**, 3356-3364, doi:10.1038/sj.emboj.7600340 (2004).
- 709 34 Adamowski, M. & Friml, J. PIN-dependent auxin transport: action, regulation, and evolution. *Plant*
710 *Cell* **27**, 20-32, doi:10.1105/tpc.114.134874 (2015).
- 711 35 Lofke, C. *et al.* Asymmetric gibberellin signaling regulates vacuolar trafficking of PIN auxin
712 transporters during root gravitropism. *Proc Natl Acad Sci U S A* **110**, 3627-3632,
713 doi:10.1073/pnas.1300107110 (2013).
- 714 36 Bennett, T. *et al.* Connective Auxin Transport in the Shoot Facilitates Communication between
715 Shoot Apices. *PLoS Biol* **14**, e1002446, doi:10.1371/journal.pbio.1002446 (2016).
- 716 37 Pasternak, T. *et al.* Protocol: an improved and universal procedure for whole-mount
717 immunolocalization in plants. *Plant Methods* **11**, 50, doi:10.1186/s13007-015-0094-2 (2015).
- 718 38 Dill, A. & Sun, T. Synergistic derepression of gibberellin signaling by removing RGA and GAI function
719 in Arabidopsis thaliana. *Genetics* **159**, 777-785, doi:10.1093/genetics/159.2.777 (2001).
- 720 39 Blakeslee, J. J. *et al.* Interactions among PIN-FORMED and P-glycoprotein auxin transporters in
721 Arabidopsis. *Plant Cell* **19**, 131-147, doi:10.1105/tpc.106.040782 (2007).
- 722 40 Jenness, M. K., Carraro, N., Pritchard, C. A. & Murphy, A. S. The Arabidopsis ATP-BINDING CASSETTE
723 Transporter ABCB21 Regulates Auxin Levels in Cotyledons, the Root Pericycle, and Leaves. *Front*
724 *Plant Sci* **10**, 806, doi:10.3389/fpls.2019.00806 (2019).
- 725 41 Kotogany, E., Dudits, D., Horvath, G. V. & Ayaydin, F. A rapid and robust assay for detection of S-
726 phase cell cycle progression in plant cells and tissues by using ethynyl deoxyuridine. *Plant Methods*
727 **6**, 5, doi:10.1186/1746-4811-6-5 (2010).
- 728 42 Olszewski, N., Sun, T. P. & Gubler, F. Gibberellin signaling: biosynthesis, catabolism, and response
729 pathways. *Plant Cell* **14 Suppl**, S61-80, doi:10.1105/tpc.010476 (2002).
- 730 43 Marhava, P. *et al.* A molecular rheostat adjusts auxin flux to promote root protophloem
731 differentiation. *Nature* **558**, 297-300, doi:10.1038/s41586-018-0186-z (2018).
- 732 44 Aloni, R. Role of auxin and gibberellin in differentiation of primary Phloem fibers. *Plant Physiol* **63**,
733 609-614, doi:10.1104/pp.63.4.609 (1979).
- 734 45 Wang, Y. *et al.* DELLA-NAC Interactions Mediate GA Signaling to Promote Secondary Cell Wall
735 Formation in Cotton Stem. *Front Plant Sci* **12**, 655127, doi:10.3389/fpls.2021.655127 (2021).

- 736 46 Bjorklund, S., Antti, H., Uddestrand, I., Moritz, T. & Sundberg, B. Cross-talk between gibberellin and
737 auxin in development of *Populus* wood: gibberellin stimulates polar auxin transport and has a
738 common transcriptome with auxin. *Plant Journal* **52**, 499-511, doi:10.1111/j.1365-
739 313X.2007.03250.x (2007).
- 740 47 Hu, J. *et al.* AUXIN RESPONSE FACTOR7 integrates gibberellin and auxin signaling via interactions
741 between DELLA and AUX/IAA proteins to regulate cambial activity in poplar. *Plant Cell*,
742 doi:10.1093/plcell/koac107 (2022).
- 743 48 Verna, C., Sawchuk, M. G., Linh, N. M. & Scarpella, E. Control of vein network topology by auxin
744 transport. *BMC Biol* **13**, 94, doi:10.1186/s12915-015-0208-3 (2015).
- 745 49 Powers, S. K. & Strader, L. C. Regulation of auxin transcriptional responses. *Dev Dyn* **249**, 483-495,
746 doi:10.1002/dvdy.139 (2020).
- 747 50 Wenzel, C. L., Schuetz, M., Yu, Q. & Mattsson, J. Dynamics of MONOPTEROS and PIN-FORMED1
748 expression during leaf vein pattern formation in *Arabidopsis thaliana*. *Plant J* **49**, 387-398,
749 doi:10.1111/j.1365-313X.2006.02977.x (2007).
- 750 51 Wang, X. *et al.* An inducible genome editing system for plants. *Nat Plants* **6**, 766-772,
751 doi:10.1038/s41477-020-0695-2 (2020).
- 752 52 Siligato, R. *et al.* MultiSite Gateway-Compatible Cell Type-Specific Gene-Inducible System for Plants.
753 *Plant Physiol* **170**, 627-641, doi:10.1104/pp.15.01246 (2016).
- 754 53 Karimi, M., Depicker, A. & Hilson, P. Recombinational cloning with plant gateway vectors. *Plant*
755 *Physiol* **145**, 1144-1154, doi:10.1104/pp.107.106989 (2007).
- 756 54 Xu, J. *et al.* A molecular framework for plant regeneration. *Science* **311**, 385-388,
757 doi:10.1126/science.1121790 (2006).
- 758 55 Wu, G., Lewis, D. R. & Spalding, E. P. Mutations in *Arabidopsis* multidrug resistance-like ABC
759 transporters separate the roles of acropetal and basipetal auxin transport in lateral root
760 development. *Plant Cell* **19**, 1826-1837, doi:10.1105/tpc.106.048777 (2007).
- 761 56 Blilou, I. *et al.* The PIN auxin efflux facilitator network controls growth and patterning in *Arabidopsis*
762 roots. *Nature* **433**, 39-44, doi:10.1038/nature03184 (2005).
- 763 57 Okushima, Y. *et al.* Functional genomic analysis of the AUXIN RESPONSE FACTOR gene family
764 members in *Arabidopsis thaliana*: unique and overlapping functions of ARF7 and ARF19. *Plant Cell*
765 **17**, 444-463, doi:10.1105/tpc.104.028316 (2005).
- 766 58 Goh, T., Joi, S., Mimura, T. & Fukaki, H. The establishment of asymmetry in *Arabidopsis* lateral root
767 founder cells is regulated by LBD16/ASL18 and related LBD/ASL proteins. *Development* **139**, 883-
768 893, doi:10.1242/dev.071928 (2012).
- 769 59 Alonso, J. M. *et al.* Genome-wide insertional mutagenesis of *Arabidopsis thaliana*. *Science* **301**, 653-
770 657, doi:10.1126/science.1086391 (2003).
- 771 60 Govindaraju, P., Verna, C., Zhu, T. & Scarpella, E. Vein patterning by tissue-specific auxin transport.
772 *Development* **147**, doi:10.1242/dev.187666 (2020).
- 773 61 Lin, R. & Wang, H. Two homologous ATP-binding cassette transporter proteins, AtMDR1 and
774 AtPGP1, regulate *Arabidopsis* photomorphogenesis and root development by mediating polar auxin
775 transport. *Plant Physiol* **138**, 949-964, doi:10.1104/pp.105.061572 (2005).
- 776 62 Idanheimo, N. *et al.* The *Arabidopsis thaliana* cysteine-rich receptor-like kinases CRK6 and CRK7
777 protect against apoplastic oxidative stress. *Biochem Biophys Res Commun* **445**, 457-462,
778 doi:10.1016/j.bbrc.2014.02.013 (2014).
- 779 63 Ursache, R., Andersen, T. G., Marhavy, P. & Geldner, N. A protocol for combining fluorescent
780 proteins with histological stains for diverse cell wall components. *Plant J* **93**, 399-412,
781 doi:10.1111/tpj.13784 (2018).
- 782 64 Van Rossum, G. a. D., Fred L. *Python 3 Reference Manual*. (CreateSpace, 2009).
- 783 65 Bradski, G. The OpenCV Library. *Dr. Dobb's Journal of Software Tools* (2000).
- 784 66 Pillow (PIL Fork) Documentation (readthedocs, 2015).
- 785 67 matplotlib/matplotlib v2.2.1 (Zenodo, 2018).
- 786 68 Harris, C. R. *et al.* Array programming with NumPy. *Nature* **585**, 357-362, doi:10.1038/s41586-020-
787 2649-2 (2020).

- 788 69 Murphy, A., Peer, W. A. & Taiz, L. Regulation of auxin transport by aminopeptidases and
789 endogenous flavonoids. *Planta* **211**, 315-324, doi:10.1007/s004250000300 (2000).
- 790 70 Noh, B., Murphy, A. S. & Spalding, E. P. Multidrug resistance-like genes of Arabidopsis required for
791 auxin transport and auxin-mediated development. *Plant Cell* **13**, 2441-2454,
792 doi:10.1105/tpc.010350 (2001).
- 793 71 Geisler, M. *et al.* TWISTED DWARF1, a unique plasma membrane-anchored immunophilin-like
794 protein, interacts with Arabidopsis multidrug resistance-like transporters AtPGP1 and AtPGP19.
795 *Mol Biol Cell* **14**, 4238-4249, doi:10.1091/mbc.e02-10-0698 (2003).
- 796 72 Livak, K. J. & Schmittgen, T. D. Analysis of relative gene expression data using real-time quantitative
797 PCR and the 2(-Delta Delta C(T)) Method. *Methods* **25**, 402-408, doi:10.1006/meth.2001.1262
798 (2001).
- 799 73 Vandesompele, J. *et al.* Accurate normalization of real-time quantitative RT-PCR data by geometric
800 averaging of multiple internal control genes. *Genome Biol* **3**, RESEARCH0034, doi:10.1186/gb-2002-
801 3-7-research0034 (2002).
- 802 74 Winter, D. *et al.* An "Electronic Fluorescent Pictograph" browser for exploring and analyzing large-
803 scale biological data sets. *PLoS One* **2**, e718, doi:10.1371/journal.pone.0000718 (2007).
- 804